IEEE Access
Multidisciplinary ⋮ Rapid Review ⋮ Open Access Journal

Received June 8, 2021, accepted June 23, 2021, date of publication June 28, 2021, date of current version July 8, 2021.

Digital Object Identifier 10.1109/ACCESS.2021.3093084

Application of a New Fusion of Flower Pollinated With Pathfinder Algorithm for AGC of Multi-Source Interconnected Power System

STEPHEN OLADIPO[1], YANXIA SUN[1], (Senior Member, IEEE), AND ZENGHUI WANG[2], (Member, IEEE)

[1]Department of Electrical and Electronic Engineering Science, University of Johannesburg, Johannesburg 2006, South Africa
[2]Department of Electrical Engineering, University of South Africa, Florida 1709, South Africa

Corresponding author: Yanxia Sun (ysun@uj.ac.za)

This work was supported in part by the South African National Research Foundation under Grant 120106 and Grant 132797, and in part by the South African National Research Foundation Incentive under Grant 132159.

ABSTRACT As the world's population grows and energy demand increases, it is necessary to increase the scale of the electrical system, which is more complicated. Consequently, adopting automatic generation control (AGC) scheme to meet the demand becomes inevitable. In this article, the fusion of flower pollinated algorithm (FPA) and pathfinder algorithm (PFA), named hereafter as *h*FPAPFA, is proposed to achieve maximum control efficiency by combining the exploitation of FPA with the exploration capacity of PFA. The proposed *h*FPAPFA is meant to regulate two unequal multi-area interconnected power system with different generating units such as thermal, hydro, wind power and diesel plants. The proposed control scheme aims to achieve this by using the new algorithm to optimize the fractional-order set-point weighted PID (FOSWPID) parameters under time domain-based fitness functions namely, integral time square error (ITSE) and integral time absolute error (ITAE) while simultaneously minimizing the power losses. Employing the same interconnected power systems, a comparative study with some recent approaches in renowned journals is conducted. The performance of the proposed method is observed under diverse load conditions scenarios. Moreover, three nonlinearities including boiler dynamics, the governor dead band (GDB) and generation rate constraints (GRC) are further integrated into the system from a pragmatic context. Finally, sensitivity tests involving various parameter changes and the introduction of random step load perturbations are carried out. From the results, the proposed approach outperformed other approaches under different load condition scenarios, incorporation of nonlinearities and random load perturbation, demonstrating the proposed technique's efficacy and reliability.

INDEX TERMS Automatic generation control (AGC), flower pollinated algorithm, pathfinder algorithm integral time absolute error, governor dead band (GDB), generation rate constraints (GRC).

I. INTRODUCTION

A. LITERATURE REVIEW

The power system is a complex system that consists of interconnected active elements. Meeting the constantly evolving demand from consumers has created huge puzzles for engineers. The top priority of power system industries is to ensure adequate generation, transmission, and electric power distribution. Given the enormous developments in technology, the need for power supply has become essential for individuals and industries [1]. The power systems are becoming more and more complicated since they include multiple sources such as biomass, fossil fuels, solar thermal energy, wind, hydro etc. The renewable energy sources have significantly contributed to the supply of energy to the power grid sectors. However, stable, and good quality power production in the power system still poses a significant challenge due to the continuous change in load. To achieve optimal power distribution to customers, the active power produced must be proportionate to the power demand;

The associate editor coordinating the review of this manuscript and approving it for publication was Siqi Bu.

otherwise, the frequency of the generating units would be adversely affected [2], [3]. When the power produced falls below the required quantity, the generator units begin to decrease in speed and frequency. The discrepancy between the power generated and the required load demand over a long time leads to an alteration in the system's nominal frequency and voltage profile [4], [5]. To tackle the effect of changes in the system's frequency and tie-line loading, the automatic generation control (AGC) control scheme is employed to regulate the deviations in active power and active power output of each generation unit within the control zone, as well as to maintain the frequency and provide interchange with other fields [6]. Hence, the primary purpose of AGC is to standardize the frequency of the system and tie-line power at a nominal value. To achieve this, several approaches have been explored in the literature, including but not limited to classical control [7], adaptive control [8], optimal control [9], robust control [10] and artificial neural network [11]. However, many modern power systems require an effective controller and more innovative optimization approaches to achieve good frequency and tie-line power stability [12]. The proportional-integral-derivative (PID) controller have been used for many industrial applications over decades [13]–[16]. This is attributable to their simple compositional structure, remarkable capabilities and many other advantages [17]–[19]. Although the PID controller is an admirable preference for many control processes, it becomes ineffective for controlling nonlinear systems, has a low noise immunity and is susceptible to parameter variations. When considering the intrinsic non-linearity of the power systems, the output of a basic proportional-integral controller degrades in terms of the overshoot and setting times of the system's frequency and tie-line power deviation [20]. Subsequently, modern control theories have made significant advances in PID control design by using the principle of fractional calculus to optimize industrial process performance [21]. The fractional-order proportional integral derivative (FOPID) controller, also known as ($PI^{\lambda}D^{\mu}$), is an improved version of the regular PID controller. One of the major outstanding performance of the FOPID is found in its two extra tunable parameters (integral order and derivative order) which can be used to enhance the performance of control loops. The FOPID efficacy is evident in its robust performance when dealing with higher order, nonlinearity and systems with delay [22]–[24]. As established in refs. [25]–[28], the FOPID control design has much more adaptability in its fine-tuning scheme and also a large area of parameters that govern the controlled system with increased reliability and stability of the control loop. However, it is essential that FOPID have a clear defining weighting mechanism to present the required optimal control structure. This will invariably lead to a stronger control scheme with clear regulation of the set-point and load control [29]. Hence, one of the motivations for this work is to design a fractional-order set-point weighted PID (FOSWPID) for the AGC system, particularly because it has rarely been applied to the AGC system. Nevertheless, it is worth mentioning that the controllers can only perform optimally if their parameters are well-tuned.

Recent approaches such as artificial intelligence (AI) and soft computing (SC) have made important strides when developing the controller architecture to solve technical challenges [30]. Many researchers have proposed the optimization of classical controllers with AI and SC techniques, especially for realizing a balance of the frequency and tie-line power deviations in the AGC system. Mohanty [31] have proposed an AGC using a moth flame optimization algorithm (MFOA) to select the parameters of the proportional-integral-double-derivative (PIDD) controller. The AGC consists of two unequal areas of the thermal system with the inclusion of GRC to reveal its dynamic stability under nonlinearities. A comparative analysis was performed under various scenarios to assess the efficacy of the proposed method. Under time-domain analysis, the proposed MFOA-based PIDD outscored other approaches. From the reports of Debbarma *et al.* [32], optimal gain control of a two-degree-of-freedom fractional order PID (2-DOF-FOPID) controller was proposed for the AGC of the power system. The gains of the controller and the R parameter selection were tuned with Firefly Algorithm (FA). The results of the simulation showed that the FA-based 2-DOF-FOPID gave superior performance compared with other methods. However, for a more realistic power system, the incorporation of more nonlinear elements such as the GDB and boiler dynamics could further show the efficacy of the proposed technique in refs [31], [32]. In [33] the Harmony Search Algorithm (HSA) was used to stabilize the AGC. To reach optimum equilibrium in frequency and tie-line power deviations, the control strategy involved the optimal configuration of the FO-PID controller's parameters using the suggested algorithm. In comparison to other approaches, the authors indicated that the HSA-based FOPID performed satisfactorily. Fitness dependent optimizer algorithm was employed in reference [34] to select the gains of a modified PID controller namely, integral proportional derivative (I-PD) controller for the AGC of two areas multi-source interconnected power system. The multi-source of the AGC is comprised of gas, hydro and reheat thermal unit. The success of the proposed approach is established with substantial improvement in settling time, overshoot and undershoot in the comparative study. Conversely, the application of the recent metaheuristic algorithm will present a more effective algorithm for selecting the parameters of the I-PD controller compared with the classical fitness dependent optimizer. Furthermore, Nizamuddin *et al.* [35], examined the performance of bacterial foraging optimization (BFO) algorithm in selecting the ideal gains of the PID controller while monitoring the discrepancy in frequency and tie-line power. The BFO-base PID results in higher efficiency compared to the optimized PID controller of the genetic algorithm (GA). Authors in [36] applied the search group algorithm (SGA) to tune the parameters of the PID controller to regulate the AGC while considering the ITAE-based performance criterion.

The proposed SGA-PID exceeded other techniques in the analysis. Considering the works in references [35], [36], the physical limitation and spontaneous load disturbance of the power system is necessary to show the efficacy of the proposed controllers. Again, Saikia *et al.* [7] conducted a comparative study between five different configurations of the PID controller. The controllers were optimized using the BFO algorithm. The results of the simulation show that integral–double derivative (IDD)-based BFO outperformed other controllers. The use of heuristic procedures to determine the optimum controller parameters can result in a better control system. Similarly, Nasiruddin [37] *et al.* designed the AGC for a two-area interconnected power system with multi-energy sources. The BFO algorithm was used to optimize the gains of the PID controller considering 1% step load disturbance in one of the control areas. The output of their study showed that the BFO-based PID surpassed the GA-based PID controller in terms of the system dynamic performance. Singh *et al.* [38] conducted a performance analysis for the AGC control system using an improved PID controller. The PID controller was enhanced via the incorporation of a filter inform of the derivative term to lessen the impact of noise in the input signal. The proposed controller was optimized using the jaya algorithm (JA). The authors reported an improved performance using the proposed techniques under different scenarios in comparison with differential evolution (DE), particle swarm optimization (PSO), needler-mead simplex (NMS), elephant herding optimization (EHO) and teaching-learning-based optimization (TLBO) algorithms. In an attempt to regulate the variation in the frequency and tie-line power of the multi-area power grid, Jagatheesan *et al.* [1] investigated the operation of the FPA algorithm for optimal PID controller gains with a 1% step load disturbance in area 1. The findings showed a better performance than with other approaches, namely GA-based PID and PSO-based PID controller under the same condition to ensure a fair comparison. Singh *et al.* [5], presented an optimal gain of a filtered PID (PID*n*) controller using symbiotic organisms search (SOS) algorithm. To investigate the output of a controller, some case studies of various load disruptions were performed in both areas with varying wind penetration levels. Results of simulation showed that the proposed SOS-PID*n* gave a superior performance for the change in frequency and tie-line power. In Reference [39], a pathfinder algorithm (PFA) was implemented with a fractional order tilt-integral-derivative (FOTID) controller for regulating the AGC with diverse source power system. Compared to conventional PID controllers and tilt-integral-derivative (TID) controllers using the same algorithm, the proposed PFA-based FOTID showed excellent results with better dynamic response for different sensitivity and robustness measures.

B. RESEARCH GAP AND MOTIVATION

Most of the above-mentioned approaches used a single algorithm to optimize the parameters of the different variants of the PID controllers for the AGC system. However, maintaining a balance between diversification (exploration of the search space) and intensification (exploitation of the search space) is a major prerequisite in presenting an effective algorithm [40]. To achieve this, two or more algorithms are hybridized to form a memetic algorithm that can identify the suitable algorithm features and mitigate the flaws of each. In this work, the flower pollinated algorithm is combined with the pathfinder algorithm to harness the global search capability and local convergence abilities of both algorithms to optimize the parameters of the FOSWPID controller for the AGC system. The flower pollinated algorithm (FPA) is a population-based algorithm that is characterized by its simplicity and flexibility. FPA tends to attain a good exploitation process. This is attributable to its unique parameter referred to as switching probability. In addition, the levy distribution facilitates the exploration of the global search towards the best solution. However, according to the operation of the FPA, the solution to the optimization problem is reliant upon interaction with pollen individuals. This has a detrimental consequence of being conveniently stuck at a local minimum [41]. Secondly, due to the application of population diversity especially with multimodal problems, FPA is highly pruned to being stuck in local optimum [42]–[45]. On the other hand, the pathfinder algorithm (PFA) is a recently proposed algorithm that mimics the characteristics of animal group social movements and the leadership system of swarms to find the best food area or prey (global optimum). By avoiding local optima, the PFA performance is competent when used for high-dimensional, dynamic, multimodal problems. However, the PFA has a weak exploitative capability. Given their respective strengths, FPA and PFA are suitable for hybridization. The mixed algorithm outperforms the individual algorithms because it identifies the appropriate algorithm features to mitigate the flaws of each one attaining a good equilibrium between intensification and diversification. This paper aims to present a hybrid of optimization-based algorithms which comprises the integration of FPA and pathfinder algorithm PFA for addressing the problems of load changes and frequency deviation in the AGC system.

C. CONTRIBUTION AND PAPER ORGANIZATION

The main contributions of this work can be explained as follows:

1) A fusion of flower pollinated algorithm (FPA) and pathfinder algorithm (PFA) is proposed for the automatic generation control system with a multi-source interconnected power system.
2) The proposed approach is applied to optimally design the fractional-order set-point weighted PID (FOSWPID) controller for a two-area multi-source interconnected AGC consisting of thermal, hydro, wind power and diesel generating units.
3) Performance comparison between the *h* FPAPFA-based FOSWPID controller over DE-PID [46], PSO-PIDD,

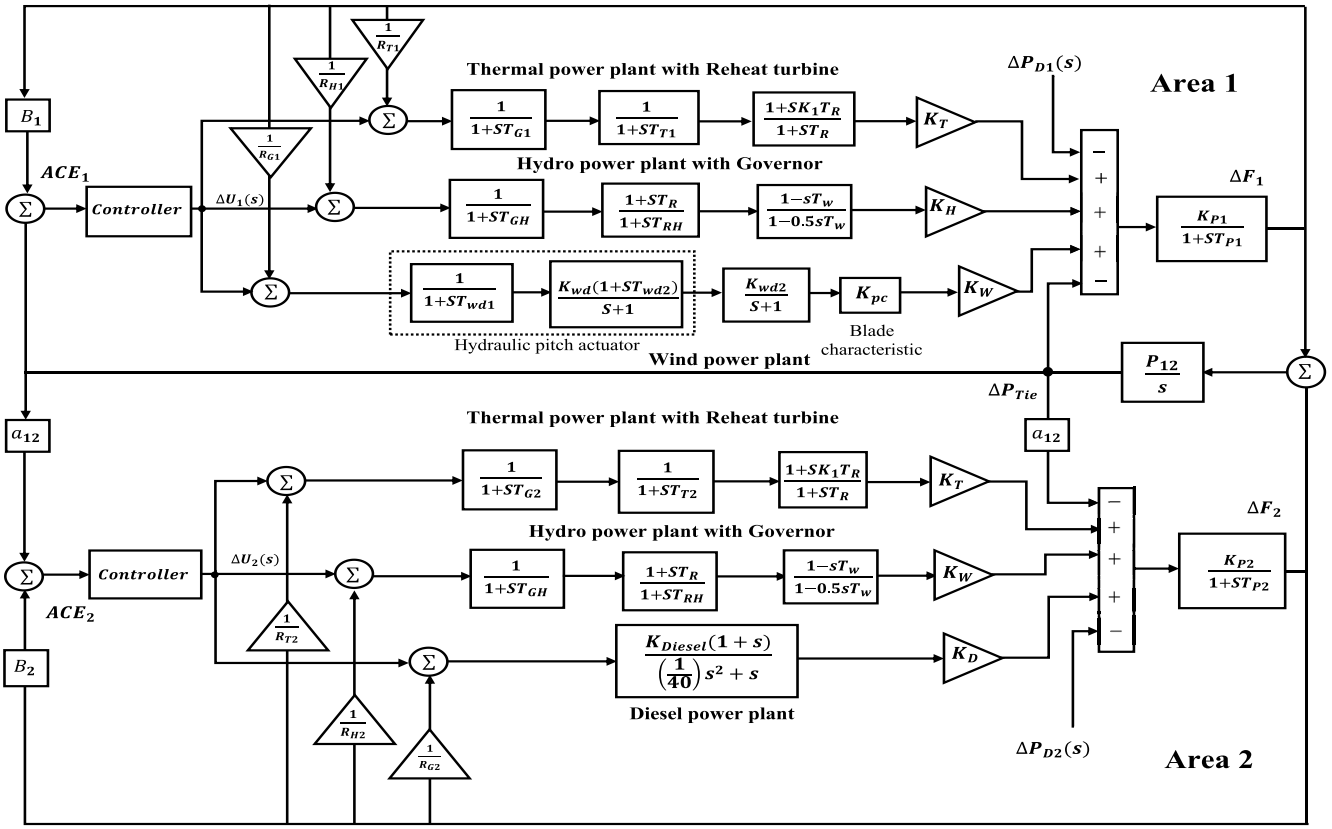

FIGURE 1. Transfer function model of two unequal areas with multi-source power system.

SOS-PID 47], SSA-TID and TLBO-PID [48] controllers while considering different load changes scenarios.

4) Sensitivity analysis is conducted to confirm the efficacy of the proposed controller under system's parameter variations, incorporating a variety of physical constraints and random load perturbations.

The organization of the rest of this paper is as follows: Section 2 describes the material and methods, followed by the control structure and the overview of the optimization techniques; Section 3 discusses the proposed algorithm; Section 4 presents the results and discussion. Finally, the conclusion is summarized in section 5.

II. MATERIAL AND METHODS

A. TWO AREA POWER SYSTEM MODEL

The fundamental objective of the AGC system is to always preserve the power system at a required nominal value in the event of load disturbance. The transfer function model of the multi-source interconnected power system is shown in Fig. 1 [46]–[48]. The system under consideration consists of two areas with different energy sources such as thermal (reheat), hydro and gas and diesel plant units. At a nominal frequency of 60Hz, each control area has a rating of 2000MW and a nominal loading of 1000MW. The two multi-source areas are connected via a tie-line. As shown in Fig. 1, the area control errors are denoted by ΔACE_1 and ΔACE_2; T_{G1} and T_{G2} are the time constants of the speed governor in seconds; T_{T1} and T_{T2} are the turbine time constant for area 1 and 2; R_{H1} and R_{G1} are the governor speed regulation parameters in p.u for area 1; the frequency bias parameters are represented by B_1 and B_2; the change in load are given as ΔPD_1 and ΔPD_2; the thermal constants are given as K_{th1} and K_{th2} respectively; P_{12} is the synchronization power coefficient, K_{GD} is the diesel turbine speed governor constant, T_D is the diesel turbine time constant; ΔF_1 and ΔF_2 are the frequency deviations in area 1 and 2 whereas ΔP_{Tie} is the marginal shift in line power (p.u). The details of all the parameters are presented in the Appendix. For a comprehensive detailed equations, readers are suggested to consult. [34], [49].

B. STRUCTURE OF THE CONTROLLER AND OBJECTIVE FUNCTION

1) FRACTIONAL-ORDER CALCULUS PRELIMINARIES

Fractional-order calculus (FOC) is a branch of mathematics that focuses on differentiation and integration of real or complex order [50]. Compared with several conventional integer techniques, the FOC has proven more suitable for analyzing and modelling real-time systems [51]. The application of FOC is expanding in many areas, including quantum mechanics, control theory, heat-flux exchange, electronics, bioengineering, chemical analysis of solutions [52]. The FOC system

is also referred to as the generalized integration and differentiation for non-integer orders and they are mathematically represented by fractional-order differential equations. The fractional-order integral-differential operator can be defined as Eq. (1) [53]

$$ {}_{\alpha}D_{t}^{r} = \begin{cases} \int_{a}^{t} (d\tau)^{-r} & \alpha < \\ 1 & \alpha = 0 \\ \dfrac{d^{r}}{dt^{r}} & \alpha > 0 \end{cases} \tag{1} $$

where ${}_{\alpha}D_{t}^{r}$, a, t and r are the fundamental operators, lower limit, upper limit, and the order of the operator. There is no unified definition of the fractional-order derivative, but there have been three generally accepted definitions, including Caputo, Grunwald-Letnikov (GL) and Riemann-Liouville (RL) [41]. Each of the three definitions has its individual properties. The Caputo definition is given in Eq. (2).

$$ {}_{\alpha}D_{t}^{r} f(t) = \frac{1}{\Gamma\,(n-r)} \int_{\alpha}^{t} \frac{f\,(\tau)}{(t-\tau)^{r-n+1}} d\tau \tag{2} $$

where $(n-1) \leq \alpha \leq n$, n is an integer, α is the real number and $\Gamma\,(.)$ is an Euler function. Furthermore, the Grunwald-Letnikov definition can be represented as Eq. (3)

$$ {}_{\alpha}D_{t}^{r} f(t) = \lim_{h \to 0} h^{-r} \,(-1)^{j} \binom{r}{j} f(t-jh) \tag{3} $$

where α and t are the lower and upper limit of the integration respectively, $\binom{r}{j}$ represents the binomial coefficient. Depending on the integration or differentiation, the value of r can either be negative or positive. The Reimann-Liouville (RL) is the simplest and most basic form of fractional-order derivative definition. It is defined as Eq. (4)

$$ {}_{\alpha}D_{t}^{r} f(t) = \frac{1}{\Gamma(n-r)} \left(\frac{d}{dt}\right)^{n} \int_{\alpha}^{t} \frac{f(\tau)}{(t-\tau)^{r-n+1}} d\tau \tag{4} $$

where $(n-1) \leq \alpha \leq n$, n is an integer, α is the real number and $\Gamma\,(.)$ is an Euler function. Numerous approximation approaches can directly provide the approximate s-transfer function of the fractional-order differentiator and integrator. A well-known approximation was given by Oustaloup [54] which utilizes a recursive distribution of zeros and poles. The simplified form of the Oustaloup approximation definition for the fractional-order differentiator s^{α} is presented in Eq. (5)

$$ s^{\alpha} = K \prod_{k=-N}^{N} \frac{s+\omega_{k}'}{s+\omega_{k}}, \quad \alpha > 0 \tag{5} $$

As presented in Eq. (5), K is the feature gain that is retained to provide the unit gain at 1 rad/sec. The approximate frequencies of poles and zeros are ω_{k}' and ω_{k}, respectively. N is a function of the number of poles and zeros. It should be noted that ω_{k}' and ω_{k} are the nominal pole and zero frequencies at the n^{th} instant whose values are true within the lower frequency (ω_{b}) and the high frequency (ω_{h}) of the system

The poles, zeros and gain of the filter can be recursively evaluated as:

$$ \omega_{k} = \omega_{b} \left(\frac{\omega_{h}}{\omega_{b}}\right)^{\frac{(k+N+(1+\alpha)/2}{(2N+1)}} \tag{6} $$

$$ \omega_{k}' = \omega_{b} \left(\frac{\omega_{h}}{\omega_{b}}\right)^{\frac{(k+N+(1-\alpha)/2}{(2N+1)}} \tag{7} $$

$$ K = \omega_{h}^{\alpha} \tag{8} $$

where α is the order of the differ-integration, the order of the filter is represented as $(2N+1)$. The output of a signal transiting the filter (as seen in Eq.(1)) is an approximation to the fractionally differentiated or integrated signal ${}_{\alpha}D_{t}^{r} f(t)$ [55]. In this study, the order of the filter is selected to be 5^{th} order Oustaloup's recursive approximation, and the chosen frequency range is $\{10^{-3}, 10^{3}\}$ rad/sec. In addition, Podlubny [53], proposed the most frequently used version of a fractional order PID controller which has both an integrator order (λ) and a differentiator order (μ). The transfer function in time domain is given as:

$$ u(t) = k_{p} e\,(t) + k_{i} D_{t}^{-\lambda} e\,(t) + k_{d} D_{t}^{\mu} e(t) \tag{9} $$

where k_{p} is the proportional gain; k_{i} is the integral gain, k_{d} is the derivative gain; λ is the integral order and μ is the derivative order. Taking the Laplace transform of Eq. (9) gives the continuous transfer function of the FOPID controller as described in Eq. (10)

$$ G(s) = k_{p} + \frac{k_{i}}{s^{\lambda}} + k_{d} s^{\mu} \tag{10} $$

When using the FOPID controller, it is apparent that besides the standard parameters K_{P}, K_{I} and K_{D} the additional two parameters namely, integral order λ and derivative-order μ should also be considered. To realize the complex FOPID controller, the FOMCON toolbox in MATLAB is used in this study [56], [57].

2) SETPOINT WEIGHTED FRACTIONAL ORDER PID CONTROLLER

The use of fractional order PID ($PI^{\lambda}D^{\mu}$) controller in previous works have shown that it has the potential to independently increase the system's efficiency in terms of sensitivity and responsiveness [58], [59]. However, relying solely on FOPID does not guarantee optimum results. As a result, the addition of set-point weighting parameters allows for a more stable control system [60]. In the same vein, fractional integral and differentiation offer a way to increase the likelihood of fine-tuning the controller's parameters to improve proficiency [61]–[63]. The synthesis of these two frameworks offers a basis to address the problems of the AGC system. Consequently, the FOSWPID controller is chosen in this paper for regulating the frequency deviation and tie-line power deviation in the AGC system. Following the past works on the AGC system which entails the application of PID-based controllers, the FOSWPID controller is similarly considered in this study for two unequal areas with

the multi-source power system. The block diagram of the FOSWPID controller is shown in Fig. 2. The design of the FOSWPID requires the determination of seven parameters: b and c which are the proportional and derivative set-point weighting parameters respectively, proportional gain (K_p), integral gain (K_i), derivative gain (K_d), integral order (λ) and derivative order (μ). The control signal $u(t)$ of a standard PID is a sum of P, I and D actions as described in Eq. (11)

$$u(t) = K_p e(t) + K_i \int_0^t e(t)dt + K_d \frac{d}{dt} e(t) \tag{11}$$

where K_p, K_i and K_d are proportional, integral, and derivative gains, respectively. The three control actions P, I and D are functions of error signal $e(t)$ given as

$$e(t) = r(t) - y(t) \tag{12}$$

where $r(t)$ is the reference or setpoint signal and $y(t)$ can be defined as the output signal or control signal. From Eq. (11), the control action of SWPID can be obtained by weighting proportional action with b and derivations action with c as given in Eq. (13) [29].

$$u(t) = K_p e_p(t) + K_i \int_0^t e_i(t)dt + K_d \frac{d}{dt} e_d(t) \tag{13}$$

with

$$e_p(t) = br(t) - y(t) \tag{14}$$

$$e_i(t) = r(t) - y(t) \tag{15}$$

$$e_d(t) = cr(t) - y(t) \tag{16}$$

$$u(t) = K_p(br(t) - y(t)) + K_i \int_0^t (r(t) - y(t))dt + K_d \frac{d}{dt}(cr(t) - y(t)) \tag{17}$$

where b, $c \in [0, 1]$ are the proportional and derivative set-point weights, respectively. The error associated with integral action is not weighted to avoid steady-state control error [29]. Therefore, $e(t) = e_i(t)$ as described in Eqs. (12) and (15). The Laplace transform of the control signal from Eq. (16) is given as:

$$U(s) = \left(K_p b + \frac{K_i}{s} + K_d cs\right) R(s) - \left(K_p + \frac{K_i}{s} + K_d s\right) Y(s) \tag{18}$$

The control action of SWP$I^{\lambda}D^{\mu}$ can be obtained by replacing the first-order integral and derivative actions with fractional order λ, μ as described below [29]:

$$U(s) = \left(K_p b + \frac{K_i}{s^{\lambda}} + K_d cs^{\mu}\right) R(s) - \left(K_p + \frac{K_i}{s^{\lambda}} + K_d s^{\mu}\right) Y(s) \tag{19}$$

The error inputs entering the controllers in area 1 and area 2 are expressed as:

$$ACE_1 = B_1 \Delta F_1 + \Delta P_{tie1-2,error} \tag{20}$$

$$ACE_2 = B_2 \Delta F_2 + \Delta P_{tie2-1,error} \tag{21}$$

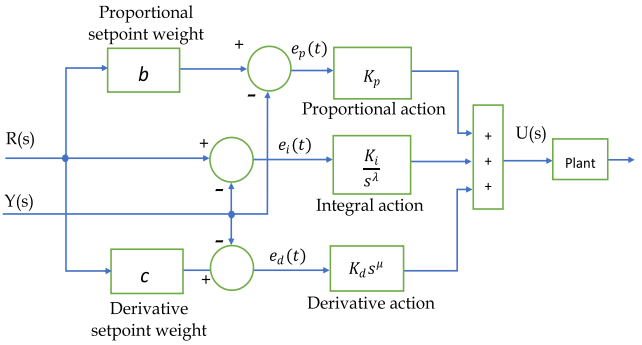

FIGURE 2. The FOSWPID control structure.

$$\Delta P_{tie2-1,error} = -\frac{P_{r1}}{P_{r2}} \Delta P_{tie2-1,error} \tag{22}$$

By considering P_{r1} and P_{r2} as the rated power of the areas,

$$a_{12} = -\frac{P_{r1}}{P_{r2}} \tag{23}$$

Then,

$$ACE_2 = B_2 \Delta F_2 + a_{12} \Delta P_{tie2-1,error} \tag{24}$$

where $\boldsymbol{\Delta F_1}$ and $\boldsymbol{\Delta F_2}$ are the frequency deviation in area 1 and area 2, respectively; $\boldsymbol{\Delta P_{tie}}$ is the change in tie-line power; $\boldsymbol{B_1}$ and $\boldsymbol{B_2}$ correspond to the frequency bias parameters.

The performance criteria can be described as a quantitative measure used to show the effectiveness of a control system [64]. A well-defined objective function reveals the device proficiency and illustrations if it satisfies the requirements of the controller's design. Findings have revealed that the performance of a typical PID controller has long been established by using some performance criterion namely, integral squared error (ISE), integral of time-weighted absolute error (ITAE), integral of time multiply squared error (ITSE) and integral of absolute error (IAE) [65]. The minimization of the fitness function is an essential procedure in attaining optimized parameters for the parameters. The ITAE has been reported to be an effective objective function for the AGC system [66], [67]. This is because of its simplicity of use, reliability and improved efficiency in outputs [68]–[70]. The ITAE criterion exceeds IAE and ISE in its ability to minimize the settling time. Nevertheless, the ITSE is well-known for its capability to impose a higher penalty on large oscillations due to its squared error, and hence successfully help to minimize large oscillations in frequency and tie-line power deviations. Hence, the proposed algorithm uses the ITSE to display the performance of controllers. The mathematical description of ITSE is given in Eq. (25) and other cost functions are defined by Eqs. (27)-(28).

$$\boldsymbol{ITSE} = \int_0^T \left((\boldsymbol{\Delta F_i})^2 + \left(\boldsymbol{\Delta P_{Tie-i-k}}\right)^2\right) \boldsymbol{tdt} \tag{25}$$

$$ITAE = \int_0^t (|\Delta F_i| + |\Delta P_{Tie-i-k}|)t dt \tag{26}$$

$$ISE = \int_0^T \left((\Delta F_i)^2 + \left(\Delta P_{Tie-i-k}\right)^2\right) dt \tag{27}$$

$$IAE = \int_0^t (|\Delta F_i| + |\Delta P_{Tie-i-k}|) dt \tag{28}$$

where t is the simulation time, ΔF_i is the frequency deviation in area i, $\Delta P_{Tie-i-k}$ is the change in tie-line power connected in-between area i and area k. The parameters of the FOSWPID controller are optimized by the proposed h FPAPFA algorithm by minimizing J according to the following constraints:

$$\begin{aligned} &Minimize\ J \\ &\qquad K_P^{min} < K < K_p^{max} \\ &\qquad K_I^{min} < K < K_I^{max} \\ &Subject\ to\ K_D^{min} < K < K_D^{max} \\ &\qquad \mu^{min} < \mu < \mu^{max} \\ &\qquad \lambda^{min} < \lambda < \lambda^{max} \\ &\qquad b^{min} < b < b^{max} \\ &\qquad c^{min} < c < c^{max} \end{aligned} \tag{29}$$

where the superscripts *min* and *max* represent the minimum and maximum values of the controller parameters, respectively. The minimum and maximum values for the gain of the controllers are within the range [0, 2] while the fractional orders of the integral and derivative terms λ and μ are within the range [0, 1]. The ranges of b and c are within [0, 1].

C. OVERVIEW OF FLOWER POLLINATED ALGORITHM

The Flower Pollinated Algorithm (FPA) is an effective segment of bio-inspired metaheuristic algorithm which replicates the pollination mechanism of flowers. Pollination can be simply put as the process of reproduction in plants. It involves the transportation of pollen grains to the receptive area of the female reproductive organ [71]. The movement is carried out by a variety of agents called pollinators. Examples of pollinators include bats, butterflies, bees, wind, water etc. Biotic pollination happens when pollination is carried out by insects or livestock. On the other hand, if the pollination agent is inanimate things such as wind and water, this is called abiotic pollination. Moreover, the process of pollination can be achieved without involving pollinators. This is called self-pollination. Self-pollination involves the transportation of pollen from the male to the female part of the same plant. One of the peculiar characteristics of the process of floral pollination is ''floral constancy.'' This is a concept that describes pollinators' preference for only visiting specific flora species while ignoring others [42]. The major significance of the concept is its guarantee of optimum pollen transfer which then stimulates and enhances flower reproduction [72].

D. MATHEMATICAL DESCRIPTION OF FPA

The FPA simulates the pollination and flower constancy functionality described above and has been modelled mathematically using four distinct rules by Yang [73]:

R1: Biotic and cross-pollination replicate the global search process which is carried out by pollinators in the similitude of Lévy flight.

R2: The local search simulates the Abiotic and self-pollination phenomenon.

R3: The flower constancy is viewed as a reproductive rate associated with the resemblance of two flowers.

R3: The operation of global pollination and local pollination are premised on switch probability $p\epsilon$ [0, 1].

At the start of the algorithm's execution, the initial population is generated randomly to determine the current best solution. The pollination class should be determined with respect to a fixed probability p which is a random number $r\epsilon$ [0, 1] to evaluate the new solution. If $rand < p$, global pollination is actualized and the expression for the flower constancy regarding *R1* and *R2* is given as:

$$x_i^{t+1} = x_i^t + \gamma L(x_i^t - gbest) \tag{30}$$

where x_i^t stands for solution i at time t, γ is the scaling factor, *gbest* is the current best solution, L is a step size which shows the tenacity of pollination, and it can be expressed as:

$$L(s, a) \sim \frac{\lambda \Gamma(\lambda) \sin(\frac{\pi\lambda}{2})}{\pi} \frac{a}{s^{1+\lambda}}, \quad s \gg s_0 > 0,\ s_0 = 0.1 \tag{31}$$

where Γ is the standard gamma function, and the distribution is effective for large steps $s > 0$. Considering the second rule i.e., when $rand > p$, the local pollination process is executed. The local pollination and flower constancy can be described as:

$$x_i^{t+1} = x_i^t + \epsilon \left(x_j^t - x_k^t\right) \tag{32}$$

where x_i^t and x_k^t are pollen from separate flowers of the same plant species, ϵ is a random number between 0 and 1. The main purpose of flower pollination is reproduction. To achieve this, the movement of the pollinators to the favourable region is a key factor. This region of the optimal solution is referred to as the global optimum and is depicted by *gbest*. Consequently, to enhance the pollination process and attain the global optimum, the basic FPA algorithm is improved by infusing the exploratory competence of the PFA algorithm. The PFA algorithm is discussed in the next session.

E. PATHFINDER ALGORITHM (PFA)

The Pathfinder Algorithm is a new algorithm that was proposed by Yapaci and Cetinkaya [74]. The PFA simulates the features of social movements of the animal group and imitates the leadership structure of the swarms to locate the best food region or prey (global optimum). The PFA consists of a population of candidate solutions known as a swarm. The proposed approach begins by arbitrarily initializing herd

members' locations. Afterwards, the fitness of each member is determined and the member's position with the best fitness is chosen as a pathfinder. The pathfinder leads the course of the remaining swarm members and navigates the search space using Eq. (36) while concurrently generating the vector of fluctuation rate (A) using Eq. (37) in every iteration. The process continues until the maximum iteration is reached. The pathfinder's function is not contingent on the group operation and this differentiates the PFA from the rest of the swarm-based algorithms and makes it exceptional [75]. To look for prey or feeding area and for following the pathfinder, the model below was proposed in [74]:

$$x_i^{K+1} = x_i^K + R_1\left(x_j^k - x_i^k\right) + R_2\left(x_p^K - x_i^k\right) + \varepsilon, \quad i \geq 2 \tag{33}$$

where the current iteration is represented by K, the position vector of the ith member is denoted as x_i, the position vector of the jth member is denoted as x_j, R_1 and R_2 are the random vectors and can be expressed as demonstrated in Eq. (34)

$$R_1 = \alpha r_1, \quad R_2 = \beta r_2 \tag{34}$$

Here, r_1 and r_2 are random variables uniformly generated in the range [0, 1], α is the interaction coefficient that determines the stability of a member along with their neighbour, and β is the attraction coefficient that sets the random distance between each member and the leader. Moreover, ε is the vector of vibration and is given as:

$$\varepsilon = \left(1 - \frac{K}{K_{max}}\right) u_1 D_{ij}, D_{ij} = \left\|x_i - x_j\right\| \tag{35}$$

where D_{ij} is the distance between two members and K_{max} is the maximum iterations. The position of the pathfinder is updated as described in Eq.(36) [74]:

$$x_p^{K+1} = x_p^K + 2r_3\left(x_p^K - x_P^{K-1}\right) + A \tag{36}$$

$$A = u_2 e^{\frac{-2K}{K_{max}}} \tag{37}$$

where u_1 and u_2 are the random vectors in the range $[-1, 1]$, and r_3 denotes the random vector uniformly generated in the range of [0, 1]. Choosing the optimal values of A and ε ensures that all the members have adequate random motion which enhances exploitation and exploration. Similarly, both α and β also enhance the exploration phase by providing a random movement of the members to get a close pathfinder in the process of finding the feeding area or the hunt.

III. THE PROPOSED HYBRID APPROACH

One of the major tasks needed for the optimal operation of metaheuristic algorithms, especially in control systems, is the achievement of adequate equilibrium between exploration (intensification) and exploitation (diversification). As mentioned earlier, each algorithm has its distinctive capabilities, which can favour exploration or exploitation [76]. As a result, when two algorithms are combined, the mixed algorithm performs better as it chooses the right algorithm attributes to improve the stability between exploration and exploitation, minimizing local minima trapping problems. Exploration ensures that the algorithm reaches the different preferred areas of the search space, while exploitation ensures the search for optimal solutions within the region. An important feature of the proposed h FPAPFA is the capability to attain a balance between exploration and exploitation. The fusion of these algorithms is essential to find the optimal solution, primarily to optimize the parameters of the FOSWPID controllers for the multi-area interconnected AGC system. Whereas FPA has the potential to exploit the search space, it falls short when it comes to exploration. The PFA, on the other hand, is a recent algorithm that is more versatile in exploration. In PFA, there is a pathfinder (global best) which leads the whole population. Two core parameters of PFA, A and ε as defined in Eqs. (34) and (37), play a key role in achieving optimum exploration by maintaining a multi-directional and random movement [74]. The PFA parameters keep on changing in each iteration and incline each member to move towards the leader. Consequently, it enables a good equilibrium between exploration and exploitation. By merging both techniques, the pollination process in FPA is combined with the pathfinder technique in such a way that the position of the FPA is updated with the equations of PFA. The description of the hFPAPFA is shown in Fig. (3) while the flowchart is described in Fig. (4).

TABLE 1. Algorithm parameters.

Algorithm	Parameter	Value
DE [46]	Mutation scaling factor, F	0.8
	Cross rate C_R	0.2
PSO	C_1	2.0
	C_2	2.0
	w_{min}	0.9
	w_{max}	0.2
SSA	NP	30
SOS [47]	NA	NA

NA- Not applicable

IV. RESULTS AND DISCUSSION

The transfer function model of the AGC of the multi-source interconnected power system under consideration is designed and simulated in MATLAB version 9.4 (R2018a) software. Thermal, hydro, wind power and diesel power plants are considered as the power sources with load demand in each area as described in Fig. 1 [34], [77]. The parameters of the proposed algorithm and other algorithms used in this study are presented in Table 1 while the optimal values of the proposed controller in comparison with others are presented in Table 2. The algorithm is executed for 50 iterations with 10 runs. The fractional-order modelling and control (FOMCON) toolbox of MATLAB [78] was employed for the fractional-order (FO) identification and controller design and optimization. The system is first subjected to different load conditions before undergoing sensitivity tests involving a variety of parameter

```
Initialize the max populations, iterations, dimensions
 Set the lower limit, upper limit and probability switch (FPA parameter)
 Find the random solution or each member within limits
 Calculate the fitness of each member and find the best solution (pathfinder)
 for i=2 to max iterations
        Define and update the PFA parameters
        update the position of pathfinder using Eq.(36) and check the bound
        for j=1 to max populations
              if rand < probability switch
                    Global pollination equations via Eq.(30)
              else
                    Local pollination equations via Eq.(32)
              endif
              Calculate the fitness of each member and find the best solution
              Update global best
              Update the positions of members using Eq. (33) and check the bound
              Calculate the fitness of each member and find the best solution
              Update global best

        endfor
 endfor
```

FIGURE 3. Pseudocode of *h*FPAPFA.

TABLE 2. Optimal parameters of the controllers.

		*h*FPAPFA-FOSWPID	SSA-TID	TLBO-PID [48]	PSO-PIDD	DE-PID [46]	SOS-PID[47]
Area 1	K_{p1}	1.7210	1.1060	0.5225	1.4290	0.2383	1.0156
	K_{i1}	0.8790	0.9145	1.9605	1.3912	0.9718	1.0204
	K_{d1}	1.0000	1.1014	1.2691	1.2679	0.4922	1.7010
	λ_1	0.9910	-	-			
	μ_1	0.9900	-	-			
	b_1	0.3879	-	-			
	c_1	0.8980	-	-			
	n_1		2.9146	-			
Area 2	K_{p2}	1.6980	0.3850	1.1090	1.8631	0.7146	0.9782
	K_{i2}	1.0000	1.1030	1.8597	1.3931	0.9918	1.1204
	K_{d2}	0.3201	1.1000	1.2793	1.3747	0.7595	1.6795
	λ_2	0.9900	-	-			
	μ_2	0.9800	-	-			
	b_2	0.4796	-	-			
	c_2	0.7889	-	-			
	n_2	-	3.120	-			

variations. Moreover, boiler dynamics, the GDB and the GRC have been incorporated into the model to demonstrate the competence of the system towards nonlinearities. The system is further subjected to a random step load perturbation while the nonlinearities are still present to further reveal its efficacy. The performances indices for the dynamic response considered are the ITSE and ITAE indexes, settling time and peak undershoot. The population size (*NP*) and the total number of iterations are 30 and 50 respectively. The parameters of the FOSWPID structured AGC system are optimized with

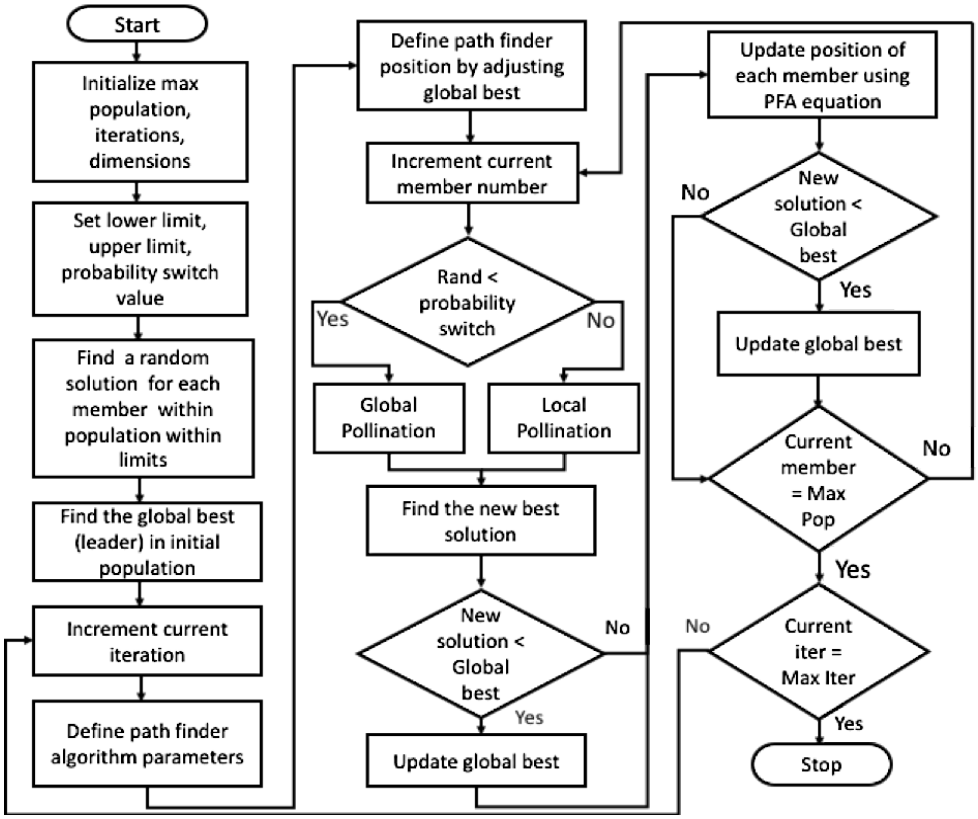

FIGURE 4. Pseudocode of *h*FPAPFA.

the proposed *h*FPAPFA and the performance is compared with the performance achieved using the techniques such as DE-PID [46], PSO-PIDD, SOS-PID [47], SSA-TID and TLBO-PID [48].

A. LOAD CHANGE SCENARIOS

The subsection describes the response of the power system under different load conditions.

1) CASE 1: A STEP LOAD INCREASE IN AREA 1 WITH NO LOAD CHANGE IN AREA 2

At the initial stage, a step load increase of 0.1 p.u is applied in area 1 with no load change in area 2. The performance of the system is observed and compared with other methods. Figs. 5(a)-(c) show the response curve obtained from the results of simulation for frequency deviations and tie-line power in both areas. As depicted in Fig. 5(a), the proposed approach yielded a more desirable response with lesser undershoot and preferable curve smoothness. Also, it is glaring from the results presented in Table 3 that the proposed *h* FPAPFA-FOSWPID offered an improved performance with the minimum value of the cost functions (ITSE = 0.0042, ITAE = 0.3064) compared with PSO (ITSE = 0.0133, ITAE = 0.6388), DE (ITSE = 0.0113, ITAE = 0.6899), SOS (ITSE = 0.0183, ITAE = 1.0860), SSA (ITSE = 0.0183, ITAE = 1.0860), TLBO (ITSE = 0.0267, ITAE = 1.0020). In terms of the dynamic response, the proposed *h* FPAPFA-FOSWPID exceeded other methods with the shortest settling time in frequency deviations compared with other techniques. Likewise, the *h* FPAPFA-FOSWPID exhibited the shortest peak undershoot compared with other methods. Consequently, better system performance is obtained with the *h* FPAPFA-FOSWPID controller as compared to other controllers in terms of lowest settling times in frequency and tie-line power variations.

2) CASE 2: A STEP LOAD INCREASE IN AREA 2 WITH NO LOAD CHANGE IN AREA 1

Figure 6(a)-(c) demonstrate the performance of the system with a step load increase of 0.1 p.u in area 2 and no-load change in area 1. With close inspection of the response curve as demonstrated graphically in Figs. 6(a)-(c), it can be established that *h* FPAPFA-FOSWPID displayed lesser damping and a quick settling time. Similarly, from Table 4 the success of the proposed *h*FPAPFA-FOSWPID is evident with the minimum peak undershoot for the frequency and tie-line power deviations in area 1 and 2 respectively. That being said, the shortest values of ITSE (0.00423) and ITAE (0.3060) is obtained by *h*FPAPFA-FOSWPID. In terms of the settling time, *h* FPAPFA-FOSWPID outscored other controllers with the least settling time (T_s = 9.8484 s) for frequency deviation in area 1, better settling time (T_s = 9.6512 s) in the frequency deviation of area 2 and finally with a settling time (T_s = 24.6530 s) in the tie-line power deviation.

TABLE 3. Performance indices of the dynamic response for case 1.

Controllers	ITSE	ITAE	Settling time (s)(T_s)			Undershoot (U_{sh})		
			ΔF_1	ΔF_2	ΔP_{tie}	ΔF_1	ΔF_2	ΔP_{tie}
PSO-PIDD	0.0133	0.6388	10.8674	27.6717	25.4707	0.0475	0.0031	0.0039
DE-PID	0.0113	0.6899	11.0654	28.3638	26.0536	0.0460	0.0028	0.0036
SOS-PID	0.0183	1.0170	9.6837	27.5964	27.3004	0.0313	0.0024	0.0033
SSA-TID	0.0287	1.0860	14.1963	27.5964	23.2524	0.0859	0.0038	0.0057
TLBO-PID	0.0267	1.0020	12.0564	29.7782	27.3070	0.0365	0.0027	0.0036
*h*FPAPFA-FOSWPID	0.0042	0.3064	9.44780	27.5039	26.4475	0.0187	0.0005	0.0005

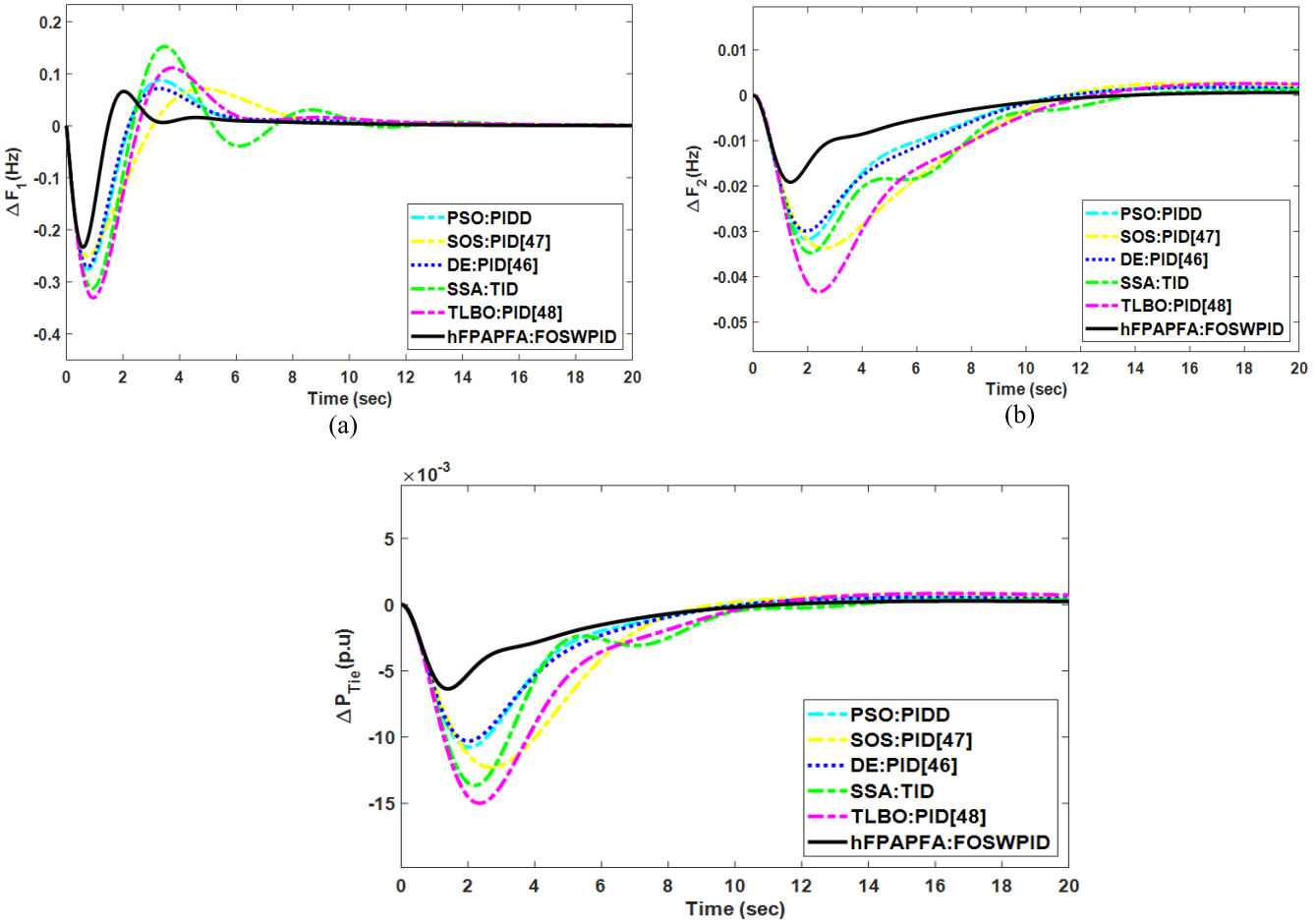

FIGURE 5. Dynamic response for case 1 (a) ΔF_1 (b) ΔF_2 (c) (a) ΔP_{tie}.

3) CASE 3: A STEP LOAD INCREASE IN AREA 1 WITH A STEP LOAD DECREASE IN AREA 2

This scenario considers a step load increase of 0.1 p.u in area 1 and a load decrease of 0.05 p.u in area 2. Figs. 7(a)-(c) display the performance of the various controllers compared with the proposed approach. From Table 5 it can be established that the proposed *h* FPAPFA-FOSWPID outscored other methods with a minimum ITSE (0.0425) and ITAE (0.3324) values. Moreover, the proposed *h*FPAPFA- FOSWPID retained its supremacy with lesser undershoot in both areas and tie-line deviations. Similarly, it delivered the shortest settling time in the frequency deviations in area 1 and tie-line deviations. Going by the results obtained in the three cases, it can be deduced that *h*FPAPFA-FOSWPID has shown excellent success in all approaches for the duo of frequency and tie-line power deviations. The corresponding values of the dynamic response for the frequency deviations and tie-line power are reported in Table 5.

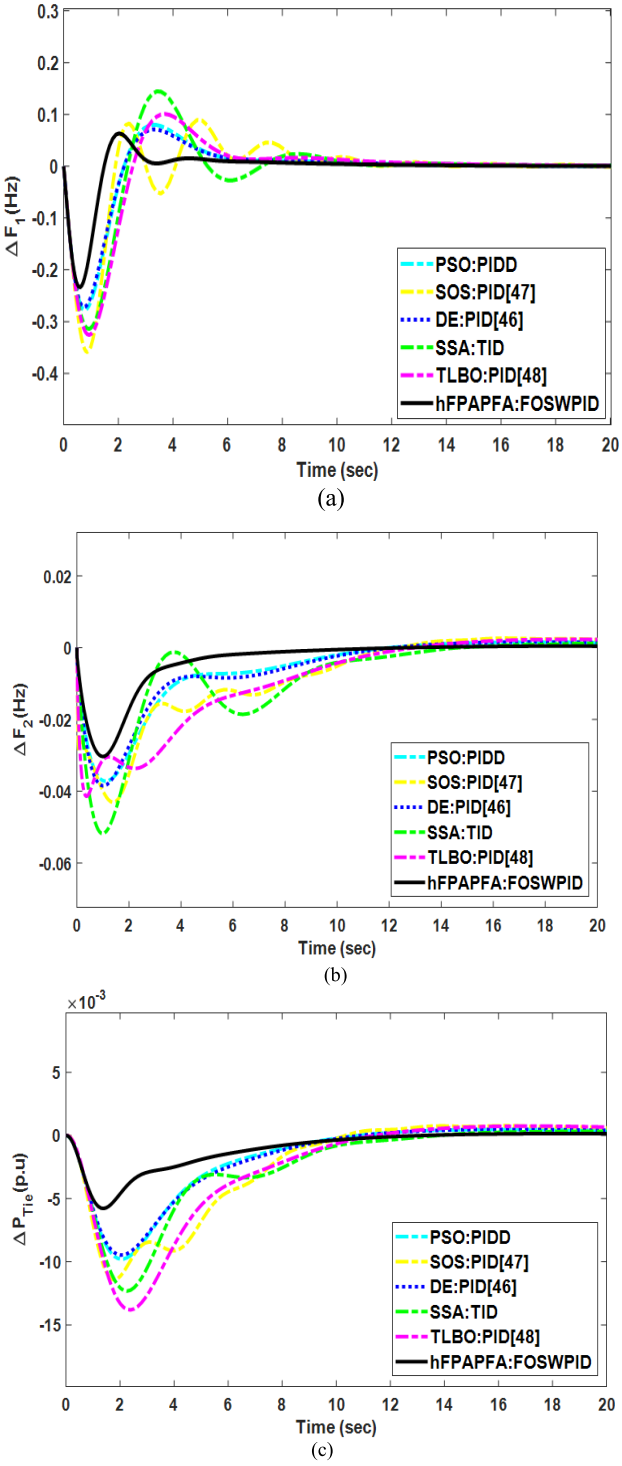

FIGURE 6. Dynamic response for case 2 (a) ΔF_1 (b) ΔF_2 (c) (a) ΔP_{tie}.

B. SENSITIVITY TEST

The fundamental aim of conducting a sensitivity analysis is to determine the system's resilience to large variations in working conditions [79]. Hence, this session is dedicated to the sensitivity test analysis of the controllers which involves varying T_G, T_T, T_R and R at the rate of $\pm 25\%$ from their nominal values without interfering with their optimal values.

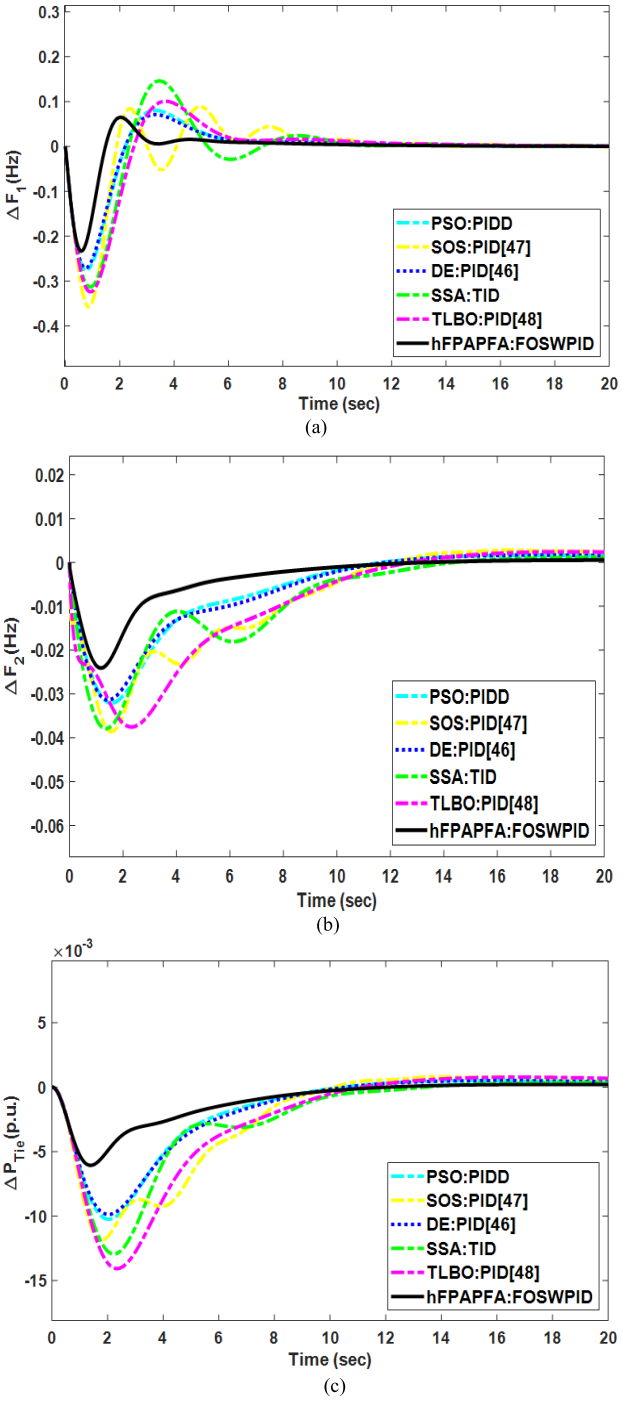

FIGURE 7. Dynamic response for case 1 (a) ΔF_1 (b) ΔF_2 (c) (a) ΔP_{tie}.

The results obtained as shown in Table 6 and Figs. (8)-(11) show a little change in the dynamic response of the controllers, within acceptable ranges which is also very close to the results obtained previously for the proposed *h*FPAPFA-FOSWPID. From a close observation of the response curve as displayed in Figs. (8)-(11), it can be inferred that the impact of the variation in the time constants has a marginal effect on the system. Consequently, it can be said that the proposed control method offers a control system that is sufficiently reliable and robust.

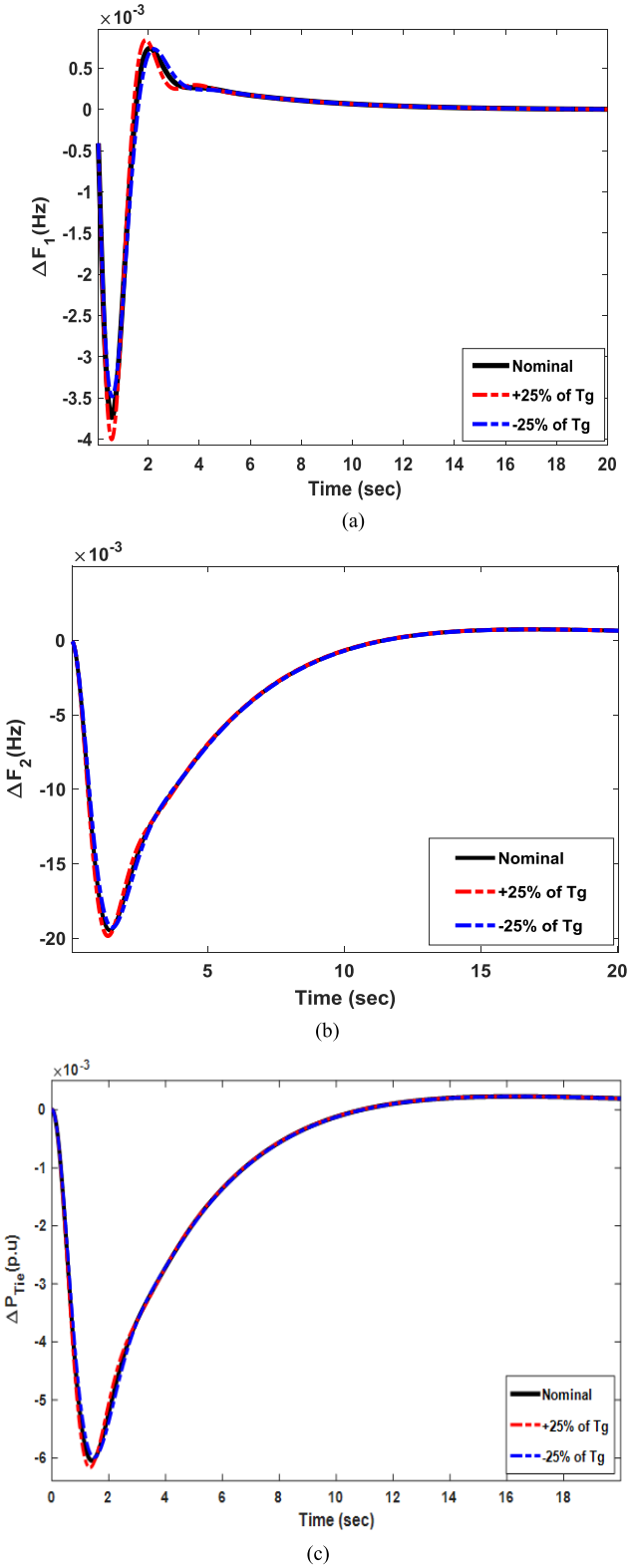

FIGURE 8. Dynamic response with variation T_G (a) ΔF_1 (b) ΔF_2 (c) ΔP_{tie}.

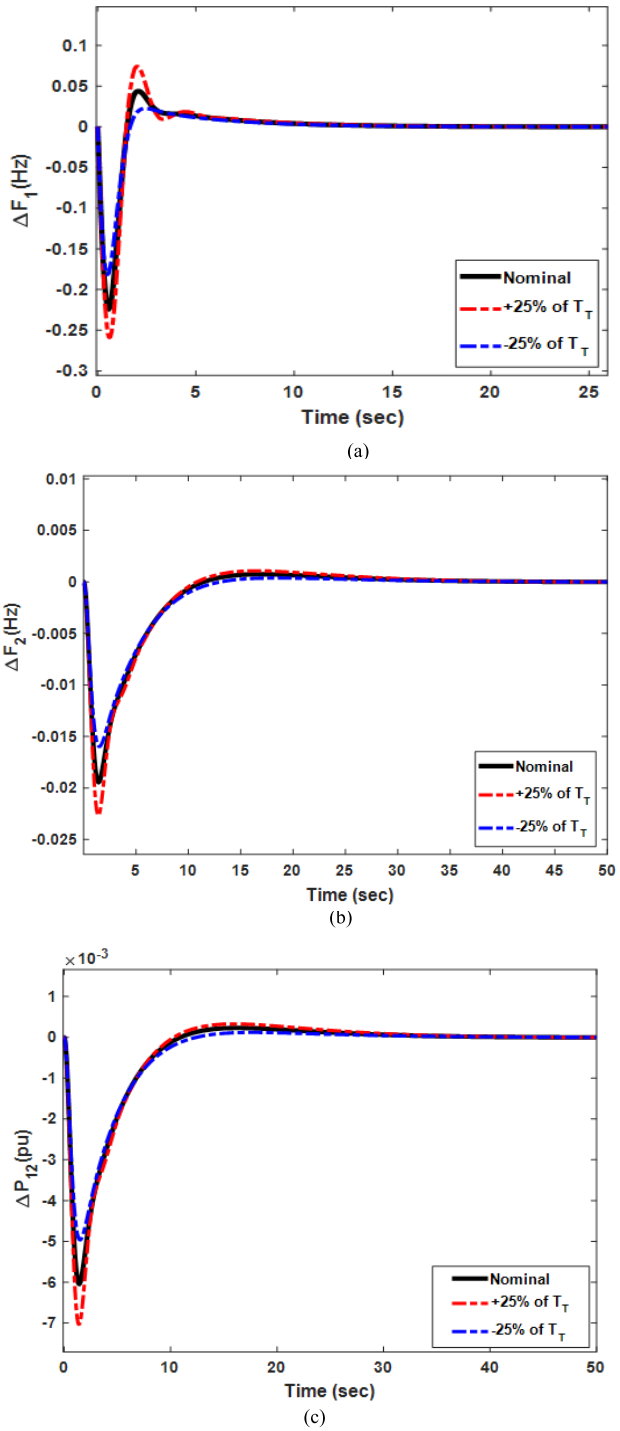

FIGURE 9. Dynamic response with variation T_T (a) ΔF_1 (b) ΔF_2 (c) (a) ΔP_{tie}.

C. INTEGRATION OF NONLINEARITIES

Investigating the system's behavior in the presence of physical limitations, also known as nonlinear components, is a necessary step to provide a reliable result from a realistic power system. Subsequently, the multi-source interconnected power system integrates boiler dynamics, Generation Rate Constant (GRC), and Governor Dead Band (GDB), which predominantly impacts the system's output. The cumulative value of an ongoing speed change, during which no position of the valve changes, is characterized as the GDB. The GDB has the features of stimulating the apparent steady-state speed

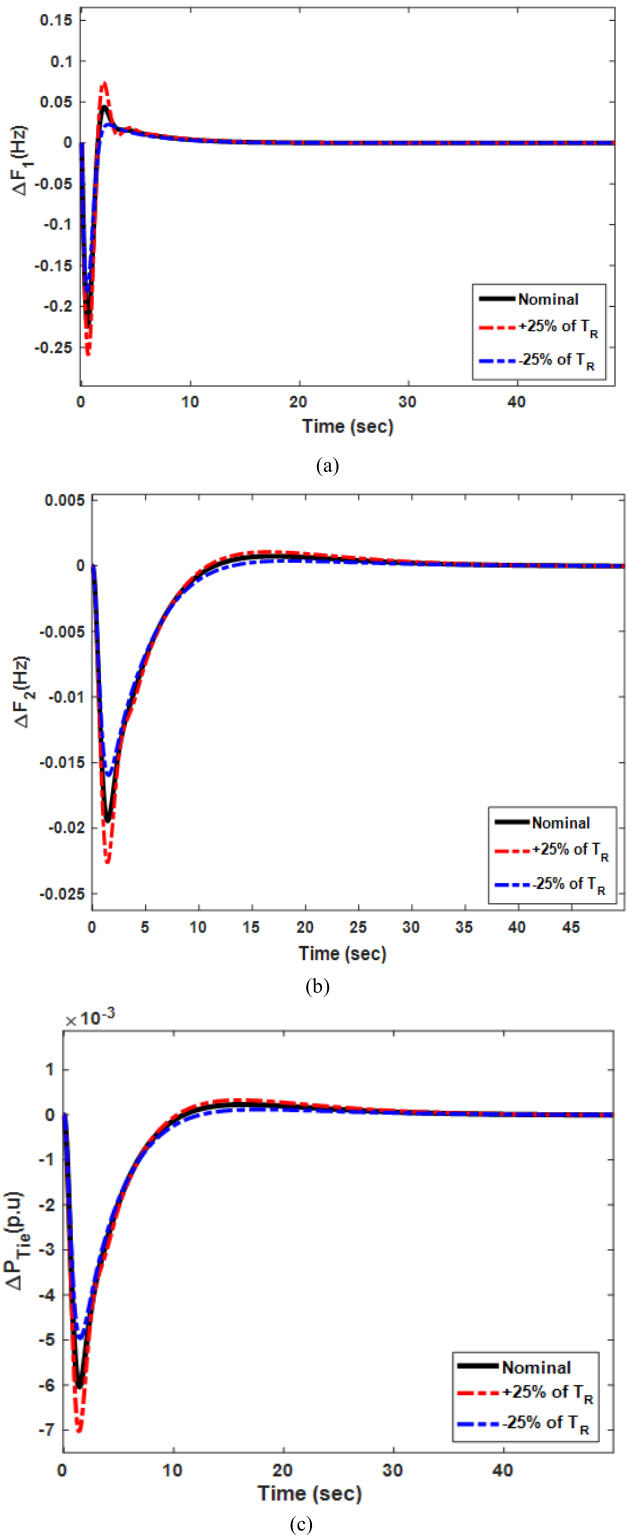

FIGURE 10. Dynamic response with variation T_R (a) ΔF_1 (b) ΔF_2 (c) ΔP_{tie}.

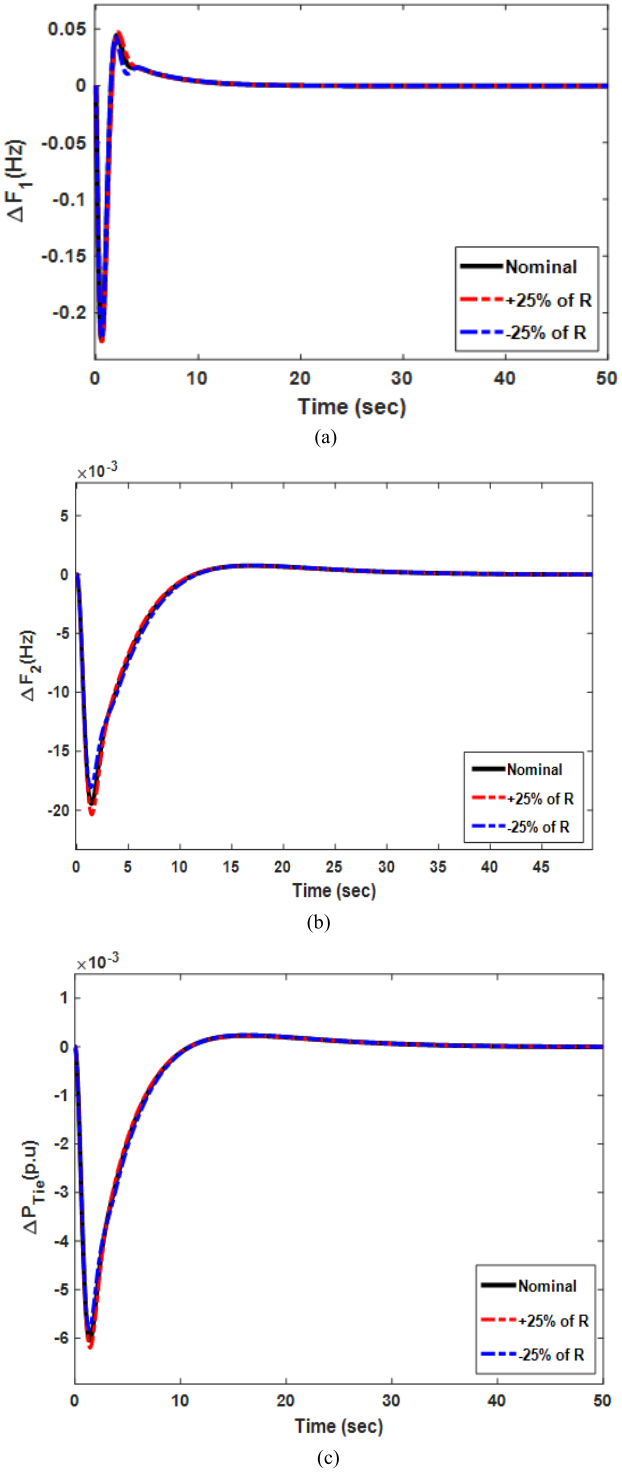

FIGURE 11. Dynamic response with variation T_R (a) ΔF_1 (b) ΔF_2 (c) ΔP_{tie}.

control, rendering the system undulating [79]. The dead band in the steam turbine is caused by the linkage that connects the piston of the servo to the camshaft. This occurrence is referred to as backlash. According to reference [48], the aforementioned operation occurs in the rack and pinion used to rotate the camshaft that is responsible for controlling the valves. The speed of the GDB has a substantial impact on the dynamic performance of the AGC system. The backlash nonlinearity effect produces a continuous sinusoidal oscillation with a natural period of about 2s [48]. As per [46], the backlash nonlinearity of 0.005% is considered at the thermal unit while 0.02% is considered in the hydro system. Furthermore, in this

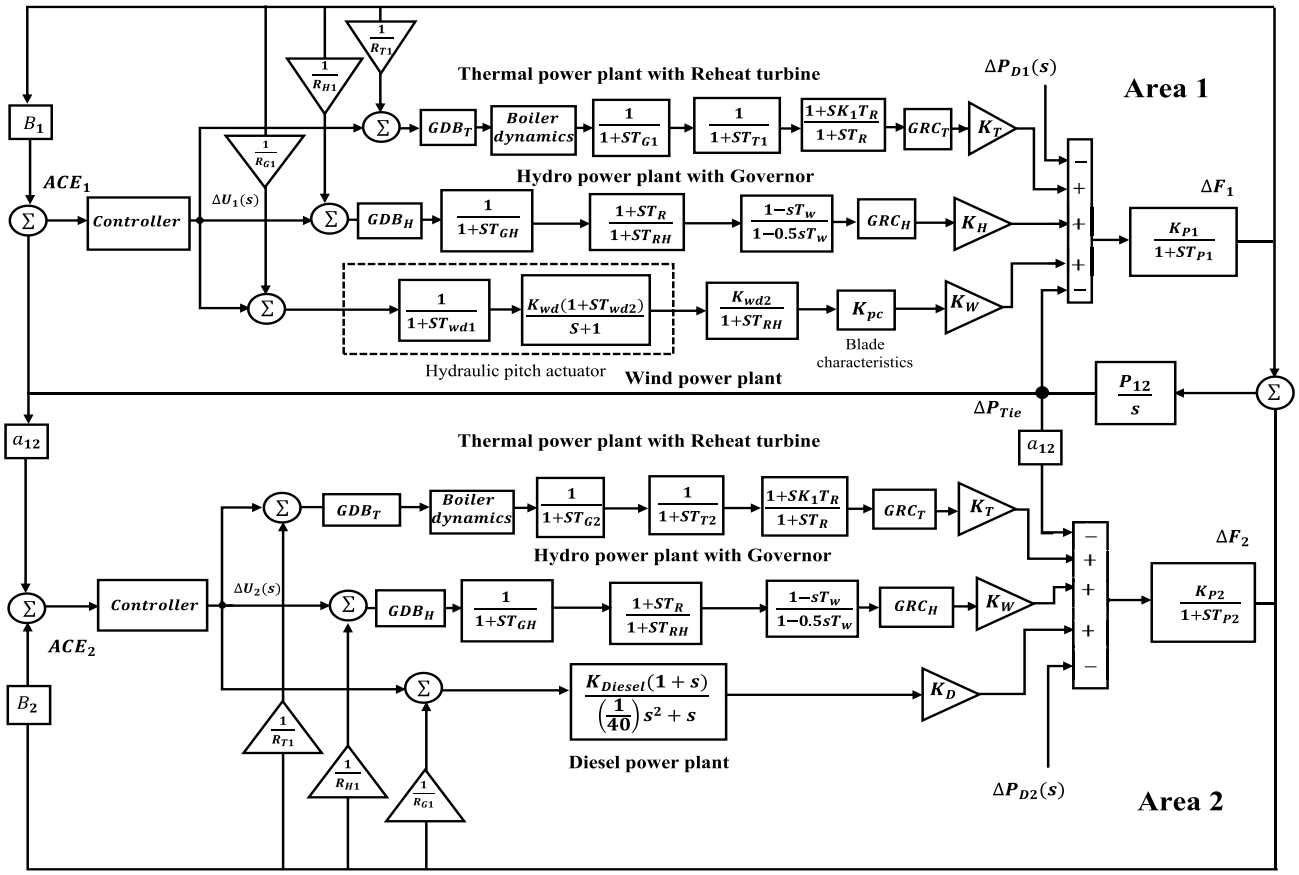

FIGURE 12. Transfer function model of two unequal areas with multi-source power system with nonlinearities.

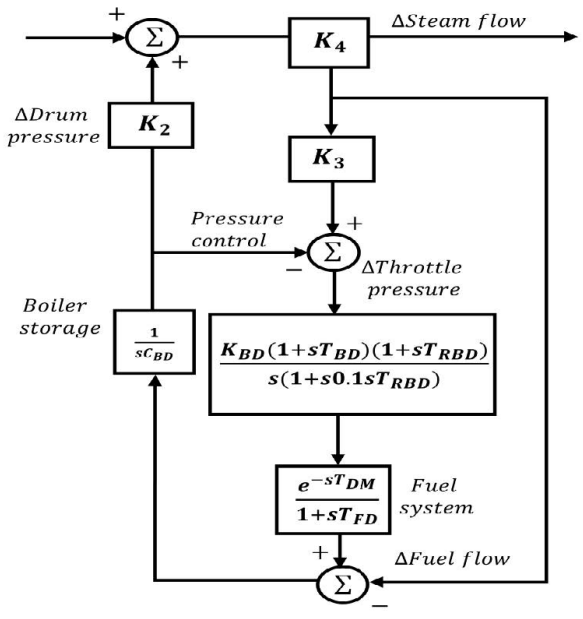

FIGURE 13. Boiler dynamics.

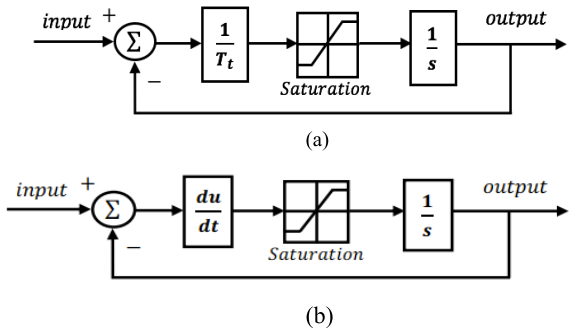

FIGURE 14. GRC in (a) thermal system (b) hydro system.

analysis, a GRC of 3% per minute is used for thermal units [46], [80]. The GRC for hydro unit is 270 per cent for raising generation per minute and 360 per cent for lowering generation per minute [81]. Fig. 12 shows the model system with the inclusion of boiler dynamics, GRC and GDB. Fig. 13 shows the boiler dynamics while Figs. 14 (a) and (b) describe the GRC in the thermal and hydro systems, respectively. The nominal parameters of the nonlinear elements are presented in the Appendix.

The dynamic responses of the nonlinear system are depicted in Figs. 15(a)-(c) representing the frequency deviation in area 1, frequency deviation in area 2 and the tie-line deviation, respectively. The proposed *h*FPAPFA-FOSWPID retained its dominance by having the smallest performance index of (ITSE = 0.01217, ITAE = 0.6150) over for PSO

TABLE 4. Performance indices of the dynamic response for case 2.

Controllers	ITSE	ITAE	Settling time (s)(T_s)			Undershoot (U_{sh})		
			ΔF_1	ΔF_2	ΔP_{tie}	ΔF_1	ΔF_2	ΔP_{tie}
PSO-PIDD	0.01264	0.7033	11.0943	26.1440	25.9944	0.0473	0.0036	0.0036
DE-PID	0.01131	0.7564	11.2712	26.1314	26.4921	0.0461	0.0037	0.0034
SOS-PID	0.02087	1.0760	10.9179	28.4369	27.9654	0.0034	0.0030	0.0024
SSA-TID	0.02616	1.2700	10.3493	22.3761	24.0902	0.0849	0.0057	0.0053
TLBO-PID	0.02393	1.0620	12.3855	29.9021	27.7502	0.0364	0.0026	0.0033
*h*FPAPFA-FOSWPID	0.00423	0.3060	9.8484	9.6512	24.6530	0.0186	4.3595e-04	2.7687e-04

TABLE 5. Performance indices of the dynamic response for case 3.

Controllers	ITSE	ITAE	Settling time (s)(T_s)			Undershoot (U_{sh})		
			ΔF_1	ΔF_2	ΔP_{tie}	ΔF_1	ΔF_2	ΔP_{tie}
PSO-PIDD	0.01261	0.7037	10.9881	27.4850	25.7356	0.0476	0.0031	0.0037
DE-PID	0.01128	0.7532	11.1815	27.9098	26.2730	0.0460	0.0030	0.0035
SOS-PID	0.01792	1.0760	10.8948	29.0197	26.7709	0.0030	0.0023	0.0027
SSA-TID	0.02638	1.1310	10.3154	26.5572	23.7530	0.0880	0.0043	0.0056
TLBO-PID	0.02376	1.0970	12.2840	30.6629	27.5860	0.0364	0.0024	0.0034
*h*FPAPFA-FOSWPID	0.00425	0.3324	9.63780	23.4881	25.7450	0.0187	4.8928e-04	3.8255e-04

TABLE 6. Sensitivity analysis for the AGC system.

Parameter Variation	%Change	Settling time $T_s(s)$			Undershoot		
		ΔF_1	ΔF_2	ΔP_{Tie}	ΔF_1	ΔF_2	ΔP_{Tie}
Nominal	0	9.6147	25.8174	25.1342	0.0114	5.9341e-04	6.1491e-04
T_G	+25	9.3236	25.6515	24.9476	0.0130	5.8636e-04	6.0813e-04
	-25	9.9155	25.9098	25.2264	0.0113	6.0078e-04	6.2198e-04
T_T	+25	9.7540	27.6130	26.8948	0.0154	7.1933e-04	7.1595e-04
	-25	9.6253	22.4005	21.8644	0.0076	8.3178e-04	8.9786e-04
T_R	+25	9.7540	27.6130	26.8948	0.0154	8.3178e-04	7.1595e-04
	-25	9.6253	22.4005	21.8644	0.0076	8.3178e-04	8.9786e-04
R	+25	9.4753	25.2167	24.7371	0.0121	5.8474e-04	6.0242e-04
	-25	9.8466	26.7589	25.7546	0.0109	6.0677e-04	6.3492e-04

(ITSE = 0.4304, ITAE = 7.0060), DE (ITSE = 0.2287, ITAE = 4.0200), SOS (ITSE = 0.3103, ITAE = 5.0720), SSA (ITSE = 0.3053, ITAE = 5.3620) and TLBO (ITSE = 0.49230, ITAE = 7.6920). In addition, *h*FPAPFA delivered an improved response by having the shortest settling time of 11.1978 s, 19.4582 s and 18.8875 s for frequency deviations in area 1, area 2 and tie-line deviation, respectively. In the same vein, its performance is evident with the least value of peak undershoot.

D. RANDOM SYSTEM LOADING

To elucidate the system's robustness the system is further subjected to random step load perturbation in all areas, as seen in Fig. 16 (a). As shown in Fig.16(b), the proposed method overtook others in terms of frequency deviation in area 1. This is apparent in the smoothness of the curve relative to others. That being said, a similar superior response is obtained in area 2. The proposed approach kept its curve smoother over time, while the others encountered

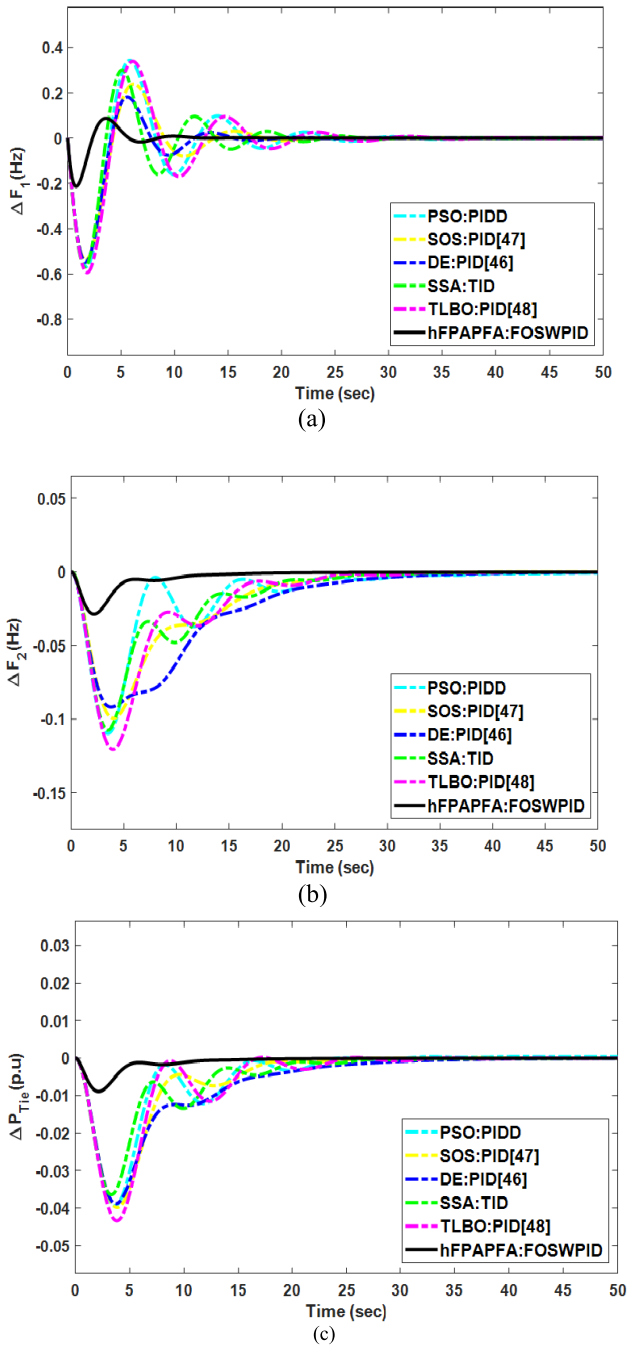

FIGURE 15. Dynamic response with nonlinearities (a) ΔF_1 (b) ΔF_2 (c) ΔP_{tie}.

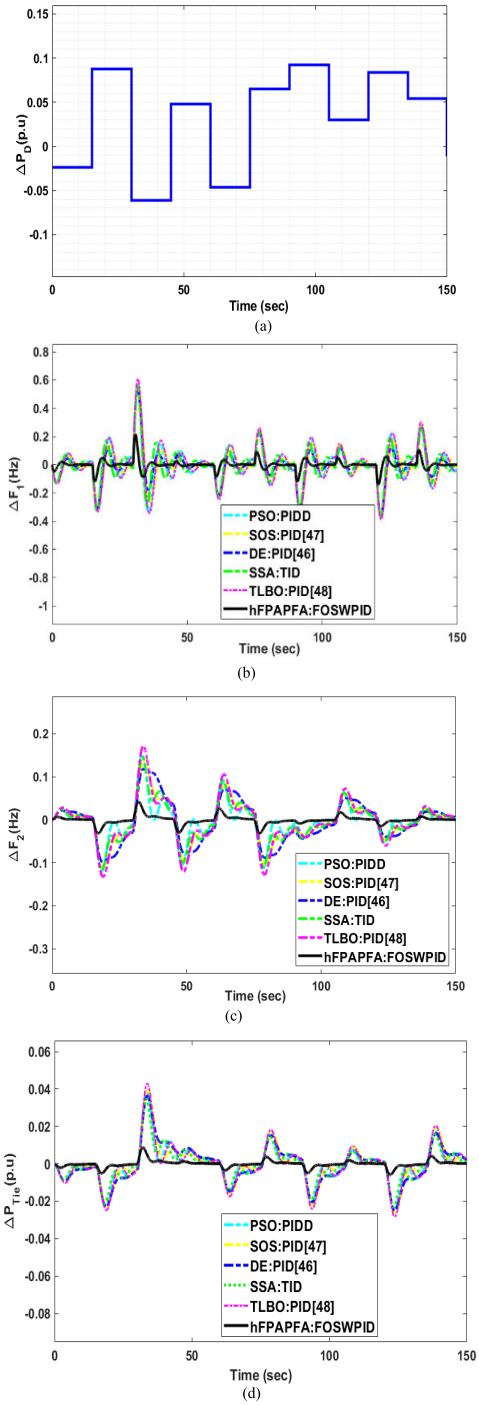

FIGURE 16. Dynamic response of the system under nonlinearities and random step load disturbance (a) random step load changes pattern (b) ΔF_1 (c) ΔF_2 (d) ΔP_{tie}.

more dampening as disclosed in Fig.16(c). Alike, the stability of the proposed approach for the tie-line power deviation is further divulged in the pattern of its curve by exhibiting the least deviant curve as shown in Fig. 16(d) compared with other methods. The responses confirmed the robustness of the proposed approach under different conditions, and this time, considering random load step perturbation. Consequently, it can be concluded that the controller is robust and effective.

V. CONCLUSION

In this work, a new algorithm based on the merger of the flower pollinated algorithm and the pathfinder algorithm is used to optimize the setpoint weighted fractional-order PID (FOSWPID) controller for the automatic generation control of a multi-source interconnected power system with renewable energy sources (thermal, hydro, wind power and

diesel plants). The system under study was examined under three load changes scenarios. For a fair comparison, the proposed approach's efficiency was examined by comparing its dynamic response with some recently published modern metaheuristic algorithms such as DE, PSO, SSA, SOS, and TLBO while subjecting them to the same multi-source interconnected power system. The results indicated that the proposed controller had a successful dynamic response compared to other controllers with minimal error criterion values, settling time and peak undershoots. Additionally, the robustness of the proposed controlling scheme is examined under different parameter variations in the range of ±25. Moreover, to further test the efficacy of the proposed algorithm three physical constraints such as boiler dynamics, GDB and GRC are incorporated into the system to be more pragmatic. The proposed approach maintained its superiority in the presence of physical constraints, confirming its efficiency. In addition, a random step load perturbation was introduced into the system under nonlinearities. By having the minimum value of the indexes namely, ITSE, ITAE, settling time and peak undershoot, the system's aggregate performance explicitly showed that the proposed algorithm generates a high-reliability response under various conditions, parameter variance, and nonlinearity effects.

In this work, we focused on a two-area power system. However, future work could be expanded to a more complex multi-source system comprised of several areas and incorporation of plug-in hybrid electric vehicles (PHEVs) for frequency stability improvement and renewable energy sources (RES). Furthermore, the proposed controller or some other control structures such as fractional order setpoint weighted cascaded controller can be designed for the study systems while employing some of the most recent optimization techniques and energy storage devices (ESS).

APPENDIX

Thermal and hydropower plant data are from Saadat [77] and Daraz *et al.* [34]. Wind and Diesel power plant are from Barisal and Mishra [82], and Das *et al.* [83]:

The nominal parameters of the system model are: $P_R = 2000MW$, $P_L = 1000MW, f = 60Hz$, $T_{G1} = 0.2$s, $T_{G2} = 0.3$s, $T_{T1} = 0.5$s, $T_{T2} = 0.5$s, $K_1 = 0.30$, $T_R = 10$s, $T_{RH} = 28.70$s, $T_{GH} = 0.2$s, $T_R = 10$s, $T_w = 1$s, $K_{pc} = 0.8$, $K_T = 0.5747$, $K_{Diesel} = 16.5$, $K_D = 0.2873$, $K_W = 0.138$, $T_{wd1} = 0.041$, $T_{wd2} = 0.6$, $K_{wd1} = 1.25$, $K_{wd2} = 1.3$, $D_1 = 0.6$, $D_2 = 0.9$, $H_1 = 5$, $H_2 = 5$, $K_{DG} = 16.5$, $T_D = 0.025$, $a_{12} = -1$, $T_p = 20$s, $P_{12} = 2$p.u, $R_{T1} = R_{H1} = R_{G1} = 0.05$ Hz/pu, $R_{T2} = R_{H2} = R_{G2} = 0.0625$; Boiler dynamics Sahu, Prusty and Panda [49]: $K_2 = 0.85$, $K_3 = 0.095$, $K_4 = 0.92$, $C_{BD} = 200$, $K_{BD} = 0.03$, $T_{BD} = 26$s, $T_{RBD} = 69$s, $T_{DM} = 0$, $T_{FD} = 10$s.

REFERENCES

[1] K. Jagatheesan, B. Anand, S. Samanta, N. Dey, V. Santhi, A. S. Ashour, and V. E. Balas, "Application of flower pollination algorithm in load frequency control of multi-area interconnected power system with nonlinearity," *Neural Comput. Appl.*, vol. 28, no. S1, pp. 475–488, Dec. 2017, doi: 10.1007/s00521-016-2361-1.

[2] O. I. Elgerd, *Electric Energy Systems Theory—An Introduction*, 2nd ed. New Delhi, India: McGraw-Hill, 2000.

[3] P. Kundur, N. J. Balu, and M. G. Lauby, *Power System Stability and Control*, vol. 7. New York, NY, USA: McGraw-Hill, 1994.

[4] H. Gozde, M. C. Taplamacioglu, and I. Kocaarslan, "Comparative performance analysis of artificial bee colony algorithm in automatic generation control for interconnected reheat thermal power system," *Int. J. Electr. Power Energy Syst.*, vol. 42, no. 1, pp. 167–178, Nov. 2012, doi: 10.1016/j.ijepes.2012.03.039.

[5] S. P. Singh, T. Prakash, and V. P. Singh, "Coordinated tuning of controller-parameters using symbiotic organisms search algorithm for frequency regulation of multi-area wind integrated power system," *Eng. Sci. Technol., Int. J.*, vol. 23, no. 1, pp. 240–252, Feb. 2020, doi: 10.1016/j.jestch.2019.03.007.

[6] D. H. Tungadio and Y. Sun, "Load frequency controllers considering renewable energy integration in power system," *Energy Rep.*, vol. 5, pp. 436–453, Nov. 2019, doi: 10.1016/j.egyr.2019.04.003.

[7] L. C. Saikia, J. Nanda, and S. Mishra, "Performance comparison of several classical controllers in AGC for multi-area interconnected thermal system," *Int. J. Electr. Power Energy Syst.*, vol. 33, no. 3, pp. 394–401, Mar. 2011, doi: 10.1016/j.ijepes.2010.08.036.

[8] M. H. Kazemi, M. Karrari, and M. B. Menhaj, "Decentralized robust adaptive-output feedback controller for power system load frequency control," *Electr. Eng.*, vol. 84, no. 2, pp. 75–83, May 2002, doi: 10.1007/s00202-001-0109-z.

[9] K. P. S. Parmar, S. Majhi, and D. P. Kothari, "Load frequency control of a realistic power system with multi-source power generation," *Int. J. Electr. Power Energy Syst.*, vol. 42, no. 1, pp. 426–433, Nov. 2012, doi: 10.1016/j.ijepes.2012.04.040.

[10] M. Azzam, "Robust automatic generation control," *Energy Convers. Manage.*, vol. 40, no. 13, pp. 1413–1421, Sep. 1999, doi: 10.1016/S0196-8904(99)00040-0.

[11] S. Bhongade, H. O. Gupta, and B. Tyagi, "Artificial neural network based automatic generation control scheme for deregulated electricity market," in *Proc. 9th Int. Power Energy Conf. (IPEC)*, Oct. 2010, pp. 1158–1163, doi: 10.1109/IPECON.2010.5696997.

[12] P. Sharma, A. Prakash, R. Shankar, and S. K. Parida, "A novel hybrid salp swarm differential evolution algorithm based 2DOF tilted-integral-derivative controller for restructured AGC," *Electr. Power Compon. Syst.*, vol. 47, nos. 19–20, pp. 1775–1790, Dec. 2019, doi: 10.1080/15325008.2020.1731870.

[13] R. Namba, T. Yamamoto, and M. Kaneda, "Robust PID controller and its application," in *Proc. IEEE Int. Conf. Syst., Man, Cybern. Comput. Cybern. Simulation*, vol. 4, Oct. 1997, pp. 3636–3641, doi: 10.1109/ICSMC.1997.633233.

[14] J. Chacón, H. Vargas, S. Dormido, and J. Sánchez, "Experimental study of nonlinear PID controllers in an air levitation system," *IFAC-PapersOnLine*, vol. 51, no. 4, pp. 304–309, 2018, doi: 10.1016/j.ifacol.2018.06.082.

[15] M. A. Khodja, C. Larbes, N. Ramzan, and A. H. Ibrahim, "Implementation of heuristical PID tuning for nonlinear system control," *Int. Rev. Autom. Control*, vol. 12, no. 2, pp. 108–114, Mar. 2019, doi: 10.15866/ireaco.v12i2.16791.

[16] S. Oladipo, Y. Sun, and Z. Wang, "Optimization of PID controller with metaheuristic algorithms for DC motor drives: Review," *Int. Rev. Electr. Eng.*, vol. 15, no. 5, pp. 352–381, Sep. 2020, doi: 10.15866/iree.v15i5.18688.

[17] Š. Bucz and A. Kozáková, "Advanced methods of PID controller tuning for specified performance," in *PID Control for Industrial Processes*. Rijeka, Croatia: InTech, 2018, pp. 73–119.

[18] A. Sungthong and W. Assawinchaichote, "Particle swam optimization based optimal PID parameters for air heater temperature control system," *Procedia Comput. Sci.*, vol. 86, pp. 108–111, Jan. 2016, doi: 10.1016/j.procs.2016.05.027.

[19] C.-T. Chao, N. Sutarna, J.-S. Chiou, and C.-J. Wang, "An optimal fuzzy PID controller design based on conventional PID control and nonlinear factors," *Appl. Sci.*, vol. 9, no. 6, p. 1224, Mar. 2019, doi: 10.3390/app9061224.

[20] K. S. Rajesh, S. S. Dash, and R. Rajagopal, "Hybrid improved firefly-pattern search optimized fuzzy aided PID controller for automatic generation control of power systems with multi-type generations," *Swarm Evol. Comput.*, vol. 44, pp. 200–211, Feb. 2019, doi: 10.1016/j.swevo.2018.03.005.

[21] R. Pradhan, S. K. Majhi, J. K. Pradhan, and B. B. Pati, "Optimal fractional order PID controller design using ant lion optimizer," *Ain Shams Eng. J.*, vol. 11, pp. 281–291, Nov. 2019, doi: 10.1016/j.asej.2019.10.005.

[22] C. A. Monje, Y. Chen, B. M. Vinagre, D. Xue, and V. Feliu-Batlle, *Fractional-Order Systems and Controls: Fundamentals and Applications*. New York, NY, USA: Springer, 2010.

[23] P. Shah and S. Agashe, "Review of fractional PID controller," *Mechatronics*, vol. 38, pp. 29–41, Sep. 2016, doi: 10.1016/j.mechatronics.2016.06.005.

[24] N. Kumar, B. Tyagi, and V. Kumar, "Deregulated multiarea AGC scheme using BBBC-FOPID controller," *Arabian J. Sci. Eng.*, vol. 42, no. 7, pp. 2641–2649, Jul. 2017, doi: 10.1007/s13369-016-2293-1.

[25] D. Xue, C. Zhao, and Y. Chen, "Fractional order PID control of a DC-motor with elastic shaft: A case study," in *Proc. Amer. Control Conf.*, 2006, pp. 3182–3187, doi: 10.1109/acc.2006.1657207.

[26] Y. Luo and Y. Chen, "Stabilizing and robust fractional order Pi controller synthesis for first order plus time delay systems," *Automatica*, vol. 48, no. 9, pp. 2159–2167, Sep. 2012, doi: 10.1016/j.automatica.2012.05.072.

[27] A. Jegatheesh and C. A. Kumar, "Novel fuzzy fractional order PID controller for non linear interacting coupled spherical tank system for level process," *Microprocessors Microsyst.*, vol. 72, Feb. 2020, Art. no. 102948, doi: 10.1016/j.micpro.2019.102948.

[28] M. Čech and M. Schlegel, "Computing PID tuning regions based on fractional-order model set," *IFAC Proc. Volumes*, vol. 45, no. 3, pp. 661–666, 2012, doi: 10.3182/20120328-3-it-3014.00112.

[29] K. Bingi, R. Ibrahim, M. N. Karsiti, and S. M. Hassan, "Fractional order set-point weighted PID controller for pH neutralization process using accelerated PSO algorithm," *Arabian J. Sci. Eng.*, vol. 43, no. 6, pp. 2687–2701, Jun. 2018, doi: 10.1007/s13369-017-2740-7.

[30] N. C. Patel, B. K. Sahu, D. P. Bagarty, P. Das, and M. K. Debnath, "A novel application of ALO-based fractional order fuzzy PID controller for AGC of power system with diverse sources of generation," *Int. J. Electr. Eng. Educ.*, vol. 58, pp. 1–23, Feb. 2019, doi: 10.1177/0020720919829710.

[31] B. Mohanty, "Performance analysis of moth flame optimization algorithm for AGC system," *Int. J. Model. Simul.*, vol. 39, no. 2, pp. 73–87, Apr. 2019, doi: 10.1080/02286203.2018.1476799.

[32] S. Debbarma, L. C. Saikia, and N. Sinha, "Automatic generation control using two degree of freedom fractional order PID controller," *Int. J. Electr. Power Energy Syst.*, vol. 58, pp. 120–129, Jun. 2014, doi: 10.1016/j.ijepes.2014.01.011.

[33] A. Behera, T. K. Panigrahi, and A. K. Sahoo, "A FO-PID controlled automatic generation control of multi area power systems tuned by harmony search," *Recent Adv. Electr. Electron. Eng., Formerly Recent Patents Electr. Electron. Eng.*, vol. 13, no. 1, pp. 101–109, Feb. 2020, doi: 10.2174/2352096511666180719105754.

[34] A. Daraz, S. A. Malik, I. U. Haq, K. B. Khan, G. F. Laghari, and F. Zafar, "Modified PID controller for automatic generation control of multi-source interconnected power system using fitness dependent optimizer algorithm," *PLoS ONE*, vol. 15, no. 11, Nov. 2020, Art. no. e0242428, doi: 10.1371/journal.pone.0242428.

[35] N. Hakimuddin, I. Nasiruddin, and T. S. Bhatti, "Generation-based automatic generation control with multisources power system using bacterial foraging algorithm," *Eng. Rep.*, vol. 2, no. 8, Aug. 2020, Art. no. e12191, doi: 10.1002/eng2.12191.

[36] D. Khamari, R. K. Sahu, and S. Panda, "Application of search group algorithm for automatic generation control of multi-area multi-source power systems," in *Proc. E3S Web Conf.*, vol. 87, Feb. 2019, pp. 1–6, doi: 10.1051/e3sconf/20198701005.

[37] I. Nasiruddin, T. S. Bhatti, and N. Hakimuddin, "Automatic generation control in an interconnected power system incorporating diverse source power plants using bacteria foraging optimization technique," *Electr. Power Compon. Syst.*, vol. 43, no. 2, pp. 189–199, Jan. 2015, doi: 10.1080/15325008.2014.975871.

[38] S. P. Singh, T. Prakash, V. P. Singh, and M. G. Babu, "Analytic hierarchy process based automatic generation control of multi-area interconnected power system using Jaya algorithm," *Eng. Appl. Artif. Intell.*, vol. 60, pp. 35–44, Apr. 2017, doi: 10.1016/j.engappai.2017.01.008.

[39] S. Priyadarshani, K. R. Subhashini, and J. K. Satapathy, "Pathfinder algorithm optimized fractional order tilt-integral-derivative (FOTID) controller for automatic generation control of multi-source power system," *Microsyst. Technol.*, vol. 27, no. 1, pp. 23–35, Jan. 2021, doi: 10.1007/s00542-020-04897-4.

[40] S. Arora, H. Singh, M. Sharma, S. Sharma, and P. Anand, "A new hybrid algorithm based on grey wolf optimization and crow search algorithm for unconstrained function optimization and feature selection," *IEEE Access*, vol. 7, pp. 26343–26361, 2019, doi: 10.1109/ACCESS.2019.2897325.

[41] Y. Ren, H. Li, and H.-C. Lin, "Optimization of feedforward neural networks using an improved flower pollination algorithm for short-term wind speed prediction," *Energies*, vol. 12, no. 21, p. 4126, Oct. 2019, doi: 10.3390/en12214126.

[42] A. B. Nasser, K. Z. Zamli, A. A. Alsewari, and B. S. Ahmed, "Hybrid flower pollination algorithm strategies for t-way test suite generation," *PLoS ONE*, vol. 13, no. 5, May 2018, Art. no. e0195187, doi: 10.1371/journal.pone.0195187.

[43] R. Wang, Y. Zhou, S. Qiao, and K. Huang, "Flower pollination algorithm with bee pollinator for cluster analysis," *Inf. Process. Lett.*, vol. 116, no. 1, pp. 1–14, Jan. 2016, doi: 10.1016/j.ipl.2015.08.007.

[44] H. M. Dubey, M. Pandit, and B. K. Panigrahi, "Hybrid flower pollination algorithm with time-varying fuzzy selection mechanism for wind integrated multi-objective dynamic economic dispatch," *Renew. Energy*, vol. 83, pp. 188–202, Nov. 2015, doi: 10.1016/j.renene.2015.04.034.

[45] Y. Zhou, R. Wang, and Q. Luo, "Elite opposition-based flower pollination algorithm," *Neurocomputing*, vol. 188, pp. 294–310, May 2016, doi: 10.1016/j.neucom.2015.01.110.

[46] B. Mohanty, S. Panda, and P. K. Hota, "Differential evolution algorithm based automatic generation control for interconnected power systems with non-linearity," *Alexandria Eng. J.*, vol. 53, no. 3, pp. 537–552, Sep. 2014, doi: 10.1016/j.aej.2014.06.006.

[47] D. Guha, P. K. Roy, and S. Banerjee, "Symbiotic organism search algorithm applied to load frequency control of multi-area power system," *Energy Syst.*, vol. 9, no. 2, pp. 439–468, May 2018, doi: 10.1007/s12667-017-0232-1.

[48] R. K. Sahu, T. S. Gorripotu, and S. Panda, "Automatic generation control of multi-area power systems with diverse energy sources using teaching learning based optimization algorithm," *Eng. Sci. Technol., Int. J.*, vol. 19, no. 1, pp. 113–134, Mar. 2016, doi: 10.1016/j.jestch.2015.07.011.

[49] P. C. Sahu, R. C. Prusty, and S. Panda, "Approaching hybridized GWO-SCA based type-II fuzzy controller in AGC of diverse energy source multi area power system," *J. King Saud Univ.-Eng. Sci.*, vol. 32, no. 3, pp. 186–197, Mar. 2020, doi: 10.1016/j.jksues.2019.01.004.

[50] A. Atangana and D. Baleanu, "New fractional derivatives with non-local and non-singular kernel: Theory and application to heat transfer model," *Thermal Sci.*, vol. 20, no. 2, pp. 763–769, 2016, doi: 10.2298/TSCI160111018A.

[51] M. Al-Dhaifallah, N. Kanagaraj, and K. S. Nisar, "Fuzzy fractional-order PID controller for fractional model of pneumatic pressure system," *Math. Problems Eng.*, vol. 2018, pp. 1–9, Jan. 2018, doi: 10.1155/2018/5478781.

[52] V. H. Haji and C. A. Monje, "Fractional-order PID control of a chopper-fed DC motor drive using a novel firefly algorithm with dynamic control mechanism," *Soft Comput.*, vol. 22, no. 18, pp. 6135–6146, Sep. 2018, doi: 10.1007/s00500-017-2677-5.

[53] I. Podlubny, "Fractional-order systems and PIλDμ-controllers," *IEEE Trans. Autom. Control*, vol. 44, no. 1, pp. 208–214, Jan. 1999, doi: 10.1109/9.739144.

[54] A. Oustaloup, F. Levron, B. Mathieu, and F. M. Nanot, "Frequency-band complex noninteger differentiator: Characterization and synthesis," *IEEE Trans. Circuits Syst. I, Fundam. Theory Appl.*, vol. 47, no. 1, pp. 25–39, 2000, doi: 10.1109/81.817385.

[55] I. Pan and S. Das, "Chaotic multi-objective optimization based design of fractional order PIλDμ controller in AVR system," *Int. J. Electr. Power Energy Syst.*, vol. 43, no. 1, pp. 393–407, Dec. 2012, doi: 10.1016/j.ijepes.2012.06.034.

[56] A. Tepljakov, E. Petlenkov, and J. Belikov, "FOMCON: Fractional-order modeling and control toolbox for MATLAB," in *Proc. 18th Int. Conf. Mixed Design Integr. Circuits Syst. (MIXDES)*, 2011, pp. 684–689.

[57] A. Tepljakov, E. Petlenkov, and J. Belikov, "FOMCON toolbox for modeling, design and implementation of fractional-order control systems," in *Applications in Control*. Berlin, Germany: De Gruyter, 2019, pp. 211–236.

[58] H. Rasouli and A. Fatehi, "Design of set-point weighting PIλ + dμ controller for vertical magnetic flux controller in Damavand tokamak," *Rev. Sci. Instrum.*, vol. 85, no. 12, Dec. 2014, Art. no. 123508, doi: 10.1063/1.4904737.

[59] F. Padula and A. Visioli, "Set-point weight tuning rules for fractional-order PID controllers," *Asian J. Control*, vol. 15, no. 3, pp. 678–690, May 2013, doi: 10.1002/asjc.634.

[60] A. Ates and C. Yeroğlu, "Online tuning of two degrees of freedom fractional order control loops," *Balkan J. Electr. Comput. Eng.*, vol. 4, no. 1, pp. 5–11, Mar. 2016, doi: 10.17694/bajece.52491.
[61] R. E. Gutiérrez, J. M. Rosário, and J. T. Machado, "Fractional order calculus: Basic concepts and engineering applications," *Math. Problems Eng.*, vol. 2010, pp. 1–19, Mar. 2010, doi: 10.1155/2010/375858.
[62] I. Podlubny, *Fractional Differential Equations* (Mathematics in Science and Engineering). New York, NY, USA: Academic, 1999.
[63] F. Merrikh-Bayat, N. Mirebrahimi, and M. R. Khalili, "Discrete-time fractional-order PID controller: Definition, tuning, digital realization and some applications," *Int. J. Control, Autom. Syst.*, vol. 13, no. 1, pp. 81–90, Feb. 2015, doi: 10.1007/s12555-013-0335-y.
[64] Y. K. Soni and R. Bhatt, "Simulated annealing optimized PID controller design using ISE, IAE, IATE and MSE error criteria," *Int. J. Adv. Res. Comput. Eng. Technol.*, vol. 2, pp. 1323–2337, Jul. 2013.
[65] H. Zhang and J. Wang, "Combined feedback–feedforward tracking control for networked control systems with probabilistic delays," *J. Franklin Inst.*, vol. 351, no. 6, pp. 3477–3489, Jun. 2014, doi: 10.1016/j.jfranklin.2014.02.012.
[66] U. K. Rout, R. K. Sahu, and S. Panda, "Design and analysis of differential evolution algorithm based automatic generation control for interconnected power system," *Ain Shams Eng. J.*, vol. 4, no. 3, pp. 409–421, Sep. 2013, doi: 10.1016/j.asej.2012.10.010.
[67] H. Shabani, B. Vahidi, and M. Ebrahimpour, "A robust PID controller based on imperialist competitive algorithm for load-frequency control of power systems," *ISA Trans.*, vol. 52, no. 1, pp. 88–95, Jan. 2013, doi: 10.1016/j.isatra.2012.09.008.
[68] D. E. Seborg, D. A. Mellichamp, and T. F. Edgar, *Process Dynamics and Control*, 2nd ed. Hoboken, NJ, USA: Wiley, 2004.
[69] N. Killingsworth and M. Krstić, "Auto-tuning of PID controllers via extremum seeking," in *Proc. Amer. Control Conf.*, vol. 4, 2005, pp. 2251–2256, doi: 10.1109/acc.2005.1470304.
[70] I. A. Khan, A. S. Alghamdi, T. A. Jumani, A. Alamgir, A. B. Awan, and A. Khidrani, "Salp swarm optimization algorithm-based fractional order PID controller for dynamic response and stability enhancement of an automatic voltage regulator system," *Electronics*, vol. 8, no. 12, p. 1472, Dec. 2019, doi: 10.3390/electronics8121472.
[71] D. L. Grebner, P. Bettinger, and J. P. Siry, "Ecosystem services," in *Introduction to Forestry and Natural Resources*. Amsterdam, The Netherlands: Elsevier, 2013, pp. 147–165.
[72] C. Grüter and F. L. W. Ratnieks, "Flower constancy in insect pollinators: Adaptive foraging behaviour or cognitive limitation?" *Communicative Integrative Biol.*, vol. 4, no. 6, pp. 633–636, Nov. 2011, doi: 10.4161/cib.16972.
[73] X. S. Yang, "Flower pollination algorithm for global optimization," in *Proc. Int. Conf. Unconventional Comput. Natural Comput.*, in Lecture Notes in Computer Science: Including Subseries Lecture Notes in Artificial Intelligence and Lecture Notes in Bioinformatics, vol. 7445, 2012, pp. 240–249, doi: 10.1007/978-3-642-32894-7_27.
[74] H. Yapici and N. Cetinkaya, "A new meta-heuristic optimizer: Pathfinder algorithm," *Appl. Soft Comput.*, vol. 78, pp. 545–568, May 2019, doi: 10.1016/j.asoc.2019.03.012.
[75] S. Priyadarshani, K. R. Subhashini, and J. K. Satapathy, "Pathfinder algorithm optimized fractional order tilt-integral-derivative (FOTID) controller for automatic generation control of multi-source power system," *Microsyst. Technol.*, vol. 27, pp. 1–13, Jun. 2020, doi: 10.1007/s00542-020-04897-4.
[76] C. Mageshkumar, S. Karthik, and V. P. Arunachalam, "Hybrid meta-heuristic algorithm for improving the efficiency of data clustering," *Cluster Comput.*, vol. 22, no. S1, pp. 435–442, Jan. 2019, doi: 10.1007/s10586-018-2242-8.
[77] H. Saadat, *Power System Analysis*. New York, NY, USA: McGraw-Hill, 1999.
[78] A. Tepljakov, E. Petlenkov, and J. Belikov, "FOMCON: A MATLAB toolbox for fractional-order system identification and control," *Int. J. Microelectron. Comput. Sci.*, vol. 2, no. 2, pp. 51–62, 2011.
[79] R. K. Sahu, S. Panda, and S. Padhan, "A hybrid firefly algorithm and pattern search technique for automatic generation control of multi area power systems," *Int. J. Electr. Power Energy Syst.*, vol. 64, pp. 9–23, Jan. 2015, doi: 10.1016/j.ijepes.2014.07.013.
[80] R. K. Sahu, S. Panda, and U. K. Rout, "DE optimized parallel 2-DOF PID controller for load frequency control of power system with governor deadband nonlinearity," *Int. J. Electr. Power Energy Syst.*, vol. 49, pp. 19–33, Jul. 2013, doi: 10.1016/j.ijepes.2012.12.009.
[81] S. R. Khuntia and S. Panda, "Simulation study for automatic generation control of a multi-area power system by ANFIS approach," *Appl. Soft Comput.*, vol. 12, no. 1, pp. 333–341, Jan. 2012, doi: 10.1016/j.asoc.2011.08.039.
[82] A. K. Barisal and S. Mishra, "Improved PSO based automatic generation control of multi-source nonlinear power systems interconnected by AC/DC links," *Cogent Eng.*, vol. 5, no. 1, Jan. 2018, Art. no. 1422228, doi: 10.1080/23311916.2017.1422228.
[83] D. Das, S. K. Aditya, and D. P. Kothari, "Dynamics of diesel and wind turbine generators on an isolated power system," *Int. J. Electr. Power Energy Syst.*, vol. 21, no. 3, pp. 183–189, Mar. 1999, doi: 10.1016/s0142-0615(98)00033-7.

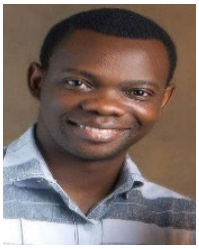

STEPHEN OLADIPO received the bachelor's and master's degrees in electronic and electrical engineering from the Ladoke Akintola University of Technology, Oyo State, Nigeria, in 2010 and 2016, respectively. He is currently pursuing the Ph.D. degree with the Department of Electrical and Electronic Engineering Science, University of Johannesburg, South Africa. His research interests include control systems, renewable energy, process control, and evolutionary algorithms. He is a member of the Council for the Regulation of Engineering in Nigeria (COREN).

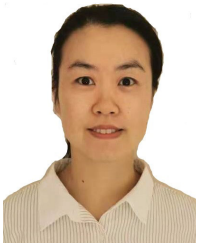

YANXIA SUN (Senior Member, IEEE) received the D.Tech. degree in electrical engineering from the Tshwane University of Technology, South Africa, and the Ph.D. degree in computer science from University Paris-EST, France, in 2012. She has 15 years of teaching and research experience. She has lectured five courses in the universities. She has supervised or co-supervised six postgraduate projects to completion. She is currently working as a Professor with the Department of Electrical and Electronic Engineering Science, University of Johannesburg, South Africa. She is the investigator or co-investigator for six research projects. She published 110 articles including 35 ISI master indexed journal articles. Her research interests include renewable energy, evolutionary optimization, neural networks, nonlinear dynamics, and control systems. She is a member of the South African Young Academy of Science (SAYAS).

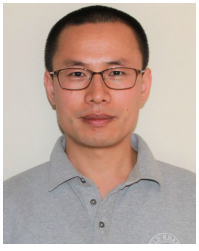

ZENGHUI WANG (Member, IEEE) received the B.Eng. degree in automation from the Naval Aviation Engineering Academy, China, in 2002, and the Ph.D. degree in control theory and control engineering from Nankai University, China, in 2007. He is currently a Professor with the Department of Electrical and Mining Engineering, University of South Africa (UNISA), South Africa. His research interests include industry 4.0, control theory and control engineering, engineering optimization, image/video processing, artificial intelligence, and chaos.